Old Dominion University

ODU Digital Commons

Winter 2011

A Microfluidic Device for Impedance Spectroscopy

Ahmet Can Sabuncu
Old Dominion University

Follow this and additional works at: https://digitalcommons.odu.edu/mae_etds

Part of the Biomedical Engineering and Bioengineering Commons, Biophysics Commons, and the Mechanical Engineering Commons

A MICROFLUIDIC DEVICE FOR IMPEDANCE SPECTROSCOPY

by

Ahmet Can Sabuncu
B. S. June 2005, Yildiz Technical University, Turkey
M. S. June 2007, Istanbul Technical University, Turkey

A Dissertation Submitted to the Faculty of
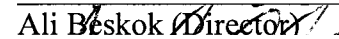Old Dominion University in Partial Fulfillment of the
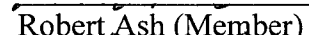Requirement for the Degree of
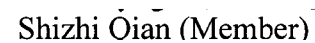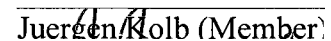
DOCTOR OF PHILOSOPHY

AEROSPACE ENGINEERING

OLD DOMINION UNIVERSITY
December 2011

Approved by:

Ali Beskok (Director)

Robert Ash (Member)

Shizhi Oian (Member)

Juergen Kolb (Member)

Michael Stacey (Member)

ABSTRACT

A MICROFLUIDIC DEVICE FOR IMPEDANCE SPECTROSCOPY

Ahmet Can Sabuncu
Old Dominion University, 2011
Director: Dr. Ali Beskok

Recently, microfluidics has become a versatile tool to investigate cellular biology and to build novel biomedical devices. Dielectric spectroscopy, on the other hand, allows non-invasive probing of biological cells. Information on the cell membrane, cytoplasm, and nucleus can be obtained by dielectric spectroscopy provided that appropriate tools are used in specific frequency ranges. This dissertation includes fabrication, characterization, and testing of a simple microfluidic device to measure cell dielectric properties. The dielectric measurements are performed on human T-cell leukemia (Jurkat), mouse melanoma (B16), mouse hepatoma (Hepa), and human costal chondrocyte cells. Dielectric measurements consist of measuring the complex impedance of cell suspensions as a function of frequency. Physical models are fitted to raw impedance data to obtain parameters for cell compartments. The dielectric measurements are further supported by dielectrophoresis (DEP) experiments. Crossover frequency, which is the applied frequency when the DEP force is equal to zero, is recorded for cells by changing buffer conductivity. Cell membrane properties are also estimated from the crossover frequency measurements. Sensing capability of the microfluidic device to external stimuli is tested with Jurkat, chondrocyte, and Hepa cells. Jurkat and chondrocyte cells are suspended in buffers with changing osmolarity, and cell membrane properties are probed. Results indicate osmotic swelling of Jurkat cells. Interestingly similar changes were not observed in chondrocyte cells. Ion efflux

from Hepa cells is quantified by conductivity measurements, and ionic flux from an average cell is calculated. Finally, a separability parameter is introduced and plotted for Jurkat and B16 cells pair. The separability parameter is based on the difference of two cells' Clausius-Mossotti factors, which is a function of the dielectric parameters of the cells, field frequency, and buffer conductivity. Using the separability maps one can choose the optimum conditions for cell separation using DEP.

To my family for all their love and understanding

Anneme, Babama ve Kardesime

ACKNOWLEDGMENTS

First of all, I would like to acknowledge the support and guidance of my major advisor for preparation of this dissertation. I would like to thank him for introducing me to the fields of which I was not aware before. I would also like to thank him for teaching me how to keep pace with the cutting edge research. Jie Zhuang taught me the major methodology of my research. I would also like to thank him for his warm friendship during the experiments that we performed together. I am in debt to him and Dr. Juergen Kolb. Dr. Michael Stacey has kindly helped me a lot by allowing me in his biology lab and teaching me about cellular biology. I learned a lot from Dr. Shizhi Qian about colloidal science, and learning from his way of conducting research was astonishing. I would like thank Dr. Richard Gordon for proof reading this dissertation and for the conversations that have broadened my view of research. I would also like to thank Dr. Robert Ash for his advice and guidance. Of course this dissertation is more valuable due to the presence of my dear family and friends. Half of the meaning of this research is hidden in my love to them and the other half my personal excitement. However, Alim's grace possesses all.

NOMENCLATURE

English Symbols

a	Radius
C	Capacitance
D	Diffusion coefficient
Du	Dukhin number
$\overline{E}$	Electric field
$\overline{d}$	Distance vector
$\hat{d}$	Dipole coefficient
e	Electronic charge
f_{CM}	Clausius-Mossotti Factor
G	Conductance
J	Ionic flux
k	Boltzmann Constant
n	Number concentration
N	Normalization parameter
$\overline{p}$	Dipole moment
p	Volume fraction
S	Separability parameter

Q, q	Charge
u	Potential Energy
$\overline{T}$	Torque
T	Temperature
t	Time
$\overline{v}$	Velocity vector
z	Valency
Z	Impedance
r, θ	Components of cylindrical coordinates

Greek Symbols

α	Low frequency double layer polarization
β	Interfacial polarization
ε_o	Vacuum permittivity
ε	Relative permittivity
ζ	Zeta (Electrokinetic) Potential
κ	Debye length
Λ	Molar conductivity
λ	Shape factor
σ	Conductivity

τ	Characteristic time
χ	Susceptibility
ψ	Electric potential
ω	Angular frequency

Subscripts

∞	High limiting extent
c	Cel
cyt	Cytoplasm
d	Diffuse layer
dl	Double layer
ff	Far field
i	Stern layer
m	Medium
mem	Membrane
p	Particle
rel	Relaxation
s	Static limit
sur	Surface
sus	Suspension

t	Total
tan	Tangential

Superscripts

~	Complex variables
*	Complex variables
'	Real part
"	Imaginary Part

TABLE OF CONTENTS

Page

LIST OF TABLES

LIST OF FIGURES

CHAPTER 1

INTRODUCTION

Dielectric properties of cells can reveal important information on cells. For instance, cell membrane thickness can be estimated by measuring cell suspension impedance. Otherwise, one has to use an electron microscope, carefully fix and section cells in order to measure cell membrane thickness. Dielectric measurements are very rapid (less than 1 second) by utilization of modern equipment that can work either in the time or frequency domain. Various quantities for cells, such as membrane capacitance and conductance, are also measurable by dielectric spectroscopy. Consequently, one can have instantaneous measurements of cellular compartments using dielectric spectroscopy provided a physical model is available. On the other hand, microfluidics that deals with manipulation of minute amounts of fluids can provide a versatile platform for dielectric spectroscopy. Through the interplay of microfluidics and dielectric spectroscopy, cells can be individually addressed and external conditions can be fine-tuned for dielectric measurements.

Cellular heterogeneity is an important feature in nature; key functions of a cell, such as cell division and apoptosis occur differently for each individual cell. In other words, each individual cell's response in an organism to a certain stimulus varies. Even if any two individuals of a cell line are genetically identical, the phenotype of individuals may vary. Recently, individual cells were shown to have stochastic gene expression that would lead to rapid change in phenotype. Stochastic switching between phenotype states may have a great impact on evolution. For instance, stochastic switching between phenotype states

might be important for microbial resistance to antibody treatment (Zhuravel and Kaern, 2005). Several reviews report on the significance of measurement of single cell dynamics (Levsky and Singer, 2003; Zhuravel and Kaern, 2005; Spiller et al., 2010). Furthermore, culturing conditions of over 99% of environmental microbes are not known. Single cell platforms, which are able to trap and investigate single microbes, can be used to find optimum culture conditions of microbial cell lines.

Microfluidics can offer a broad platform that will allow multi-parameter measurement and manipulation of cells. For instance, a biological cell can be cultured in a capture site; optical observation and dielectric spectroscopy can be done *in situ* following a stimulus. In a microfluidic system, a single cell can also be trapped to have long term gene expression measurements. Multiple measurements from single cells can allow observation of the stochastic nature of single cells. Moreover, the reduced number of cells for a microfluidic environment would be economically ideal. Usually measurement volumes in conventional dielectric spectroscopy devices are several orders of magnitude higher than the volumes used in microfluidic devices.

In this dissertation, a microfluidic device is developed to measure dielectric response of a small number of cells. Numerical models are developed to derive quantitative information on cells. Dielectric properties of three cell lines are measured by the device. The device is also shown to sense cells' response to changing medium osmolarity. The ionic efflux from the cells that are suspended in low conductivity media is quantified by impedance measurements. The dielectric responses of cells are compared with dielectrophoretic (DEP) responses. There should be a proper relationship between the cell

dielectric spectrum and cell motion under non-uniform electric fields, which is known as dielectrophoresis.

In the first part of this work an introduction to dielectric spectroscopy is given. A literature survey of recent studies on microfluidic dielectric spectroscopy is also given. Second, basic dielectric theory and details on particle polarization are addressed. In the materials and methods section, fabrication and calibration of the microfluidic device, and the procedure for modeling the measurement data is addressed. Dielectric responses of four different cell lines are given in the results and discussion part. The dissertation ends with conclusions and future work.

1.1   Dielectric Spectroscopy

There are several techniques available for dielectric probing of cells that are patch clamp, optical techniques, electromechanical techniques, and dielectric spectroscopy (Pakhomov et al., 2007; Hibino et al., 1991; Burt et al., 1990; Asami et al., 1996). Among them patch clamp is an invasive technique, and optical methods require extensive labor (Hibino et al., 1993). In addition, dielectric properties of intracellular compartments cannot be measured by optical techniques. On the other hand, dielectric spectroscopy and methods dependent on electromechanics of cells can provide detailed information of cells in a noninvasive manner.

In dielectric spectroscopy a small voltage is applied to a cell suspension, and the resulting current is measured. The measurement can be performed in the frequency or time domain (Kaatze and Feldman, 2006). The measured impedance spectrum is processed to account for lead, stray, and geometric effects that are present in the measurement system. The

resulting data is then fitted to physical models and dielectric properties of cell compartments are thereby determined. Several studies investigated dielectric responses of various cell types, such as cancer cells (Polevaya et al., 1999b; Ermolina et al., 2001) and bacteria (Carstensen, 1967; Carstensen and Marquis, 1968; van der Wal et al., 1997). While RCL (Resistance (R), Capacitance (C), and Inductance (L)) meters and impedance analyzers are used as impedance measurement devices for low frequencies, (Clarke and Gregory, 2003; Kaatze and Feldman, 2006); vector network analyzers and time domain spectrometers are used for higher frequencies (Gregory and Clarke, 2007; Kaatze and Feldman, 2006). The advantages of dielectric spectroscopy can be listed as the following: Cells can be probed in a wide frequency range, dielectric measurements are non-invasive, properties of both membrane and intracellular structures can be obtained, and small temporal resolution of dielectric spectroscopy can be used to probe cell response in real time following a stimulus. On the other hand, this technique has its own drawbacks. Electrode polarization that occurs due to the double layer formation on measurement electrodes prevents accurate resolution of low frequency behavior (Bordi et al., 2001; Feldman et al., 2001; Mazzeo and Flewitt, 2007). Usually dielectric measurements require a high volume concentration of particles, which is in turn economically undesirable as it is costly to grow a sufficient number of cells. In addition, observation of cell behavior during dielectric measurements is not possible as test fixtures are not designed for it. Finally, modeling of the measured spectra is another challenge as no physical model can precisely describe structurally complex cells.

1.1.1 Microfluidic Dielectric Spectroscopy

Dielectric measurements utilizing electromechanical behavior of cells or by microfluidic devices can address the problems of conventional dielectric spectroscopy. The electromechanical method can provide dielectric properties of cell components. It is possible to extract cell dielectric properties by measuring the crossover frequency of dielectrophoresis. However, most DEP measurements are limited to low conductivity media in order to suppress electrothermal motion, and to avoid the reduction of the electrokinetic forces. In addition, the observation of cell movements often requires long periods on the order of seconds, which precludes detection of dielectric changes in real time. On the other hand, microfluidic sytems do not suffer from these limitations, microfluidic chambers allow simultaneous functions, such as dielectric measurements on the aftermath of cell electroporation or while probing cell dynamics by fluorescent microscopy.

Earlier studies led by the pioneers of the bioimpedance field did not consider the heterogeneous nature of the cell population, and no efforts were taken to control and reduce the volume particle suspension, which was perhaps due to technological limitations. An example of historical merit, the fluidic chamber made by Fricke and Morse (Fricke and Morse, 1925) to measure impedance of blood, held 50 ml of fluid, which had to be mixed to avoid aggregation of red blood cells. Recently, development of *Lab-on-a-chip* systems that is led by the inception of new micro-technologies, has enabled impedance measurement of single cells. *Lab-on-a-chip* systems offer a platform for biochemical and electrophysiological techniques, where several simultaneous methods are otherwise not possible, such as single cell manipulation, multiparameter

measurement, and dynamic control of cellular environment. *Lab-on-a-chip* systems for improved impedance spectroscopy can be divided into two main categories: 1) Stationary systems, where cells are trapped in micro-wells and 2) Flow systems, where impedance of cells is measured as the cells flow through the device. The earliest study to measure single cell impedance can be traced back to the study led by Coulter (Coulter, 1956), where single cell DC resistance of a cell passing through a small orifice is measured by two large electrodes at the two reservoirs. A device based on this concept was named the Coulter counter, which is now commercially available. Saleh and Sohn (Saleh and Sohn, 2003) developed a Coulter counter that has a polydimethylesiloxane (PDMS) microchannel with a 200 nm constriction that is built using a micro-molding technique. Authors measured the electrical current as the DNA suspension is pushed through the constriction; DNA presence in the constriction is felt by the peaks in the current trace vs. time. Wu et al. (Wu et al., 2008) developed a system to count particles that pass between two detecting arm channels terminated by electrodes. They also incorporated a photo-detector at the sensing region in order to select fluorescent particles from the bulk flow. A recent review by Zhang et al. (Zhang et al., 2009) summarizes the advances in microfluidic particle counting, and also reports on the main limitations of microfluidic counting, such as system's low throughput. Apart from modern Coulter counters, microfluidic impedance micro-cytometry is an analog of the Coulter counter principle, where microelectrodes are embedded in the channels with small separations instead of having them at both ends of the channels. In addition, impedance measurements over a frequency range are obtained as the cells flow, which will yield more information on cells compared to the DC resistance pulses from Coulter counters. For example, Gou et al.

(Gou et al., 2011) employed 60 μm wide and 60 μm deep channels with integrated coplanar gold electrodes to discriminate normal, apoptotic, and necrotic cells by measuring the resistance and capacitance at 100 kHz. Küttel et al. (Küttel et al., 2007) discriminated parasite *Babesia bovis* infected bovine erythrocytes from uninfected and ghost erythrocytes by probing them at 8.73 MHz with coplanar electrodes. Microfluidic impedance cytometers that generally have planar or parallel electrode (Schade-Kampmann et al., 2008) designs share a common problem: identical particles flowing in a channel with slightly different positions cause fluctuations in impedance signals (Spencer and Morgan, 2011). Hydrodynamic focusing of flowing particles by inertial forces and utilization of low conductive sheath flows are generally employed in order to overcome impedance fluctuations and for increased sensitivity (Justin et al., 2011; Bernabini et al., 2011). On the other hand, stationary systems where single cells are held in hydrodynamic traps eliminate the impedance fluctuations caused by spatial variations, and such systems enable long term studies of single cells. Micro-fabricated pillars or micro-cavities with integrated electrodes generally function as hydrodynamic cell trapping sites on microfluidic platforms. Generation of chemical gradients along trapping sites or long term observation of a single cell after a certain exposure is possible with such designs. Hua and Pennell (Hua and Pennell, 2009) measured the volume change of a single cell that is exposed to a hypotonic environment by detecting electrical current changes, and simultaneously they recorded images of single cells by optical microscopy. In that study, single cells were trapped in a chevron-like structure that is in a 125 μm wide tapered section of a microfluidic channel, and a 4-electrode system was employed to measure voltage change at constant current. The authors observed 90% swelling in 1

minute following hypotonic stimuli. Chen et al. (Chen et al., 2011) proposed and tested a system that can simultaneously measure impedance and Young's modulus of single cells on a microfluidic platform. This microfluidic system consists of two layers of PDMS, where a single cell is forced to cross an aspiration channel by suction. Ag/AgCl electrodes, which have minimal electrode polarization, were employed at the inlet and outlet to measure impedance over the range 100 Hz – 1 MHz, and impedance spectrum is fit to an equivalent circuit to obtain electrical properties of cellular compartments. A microfluidic system to differentiate normal and abnormal (alcohol treated) erythrocytes at the single cell level was proposed and tested by Cho et al. (Cho et al., 2006). The authors employed twin micro-cantilever type electrodes to measure single cell impedance between 1 Hz and 10 MHz; a single red blood cell is trapped between the cantilever electrodes. According to the author's results the phase and magnitude of impedance signal differs between normal and abnormal red blood cells at frequencies up to 100 kHz. The design by Jang and Wang (Jang and Wang, 2007), which employed pillar structures and co-planar electrodes that are deposited on the channel surface, was used to measure impedance of single human cervical epithelioid carcinoma (HeLa) cells. As the measurement volume shrinks in the single cell impedance measurement chips, the effects of local variations of pH, electrical conductivity, and temperature might become dominant on the impedance signal. In order to overcome this issue, Malleo et al. (Malleo et al., 2010a) fabricated and tested a microfluidic system that consists of multiple pairs of hydrodynamic traps. The design of one pair ensured that while one trap is holding a cell, the other lacks a cell. By designing the electrodes in this manner, one electrode continuously measured the suspension impedance and served as reference; thus local

variations are reduced. The authors tested the lysing effect of surfactant Tween 20 and the toxic effect of dithiothreitol on HeLa cells by measuring the impedance at 300 kHz within the time frame of 16 minutes. One main design consideration in single cell measurements is the tight adhesion between cell and the electrode. Tight placement of cells on measurement electrodes can alter impedance measurements by decreasing the shunt current through the extracellular fluid. One may favor the usage of growth medium for long term observations, in contrast to low conductivity buffer that is commonly used for electromanipulation. Han and Frazier (Han and Frazier, 2006) overcame this issue by tightly fitting single cells into circular cavities by applying suction through a small orifice in the cavity. These authors measured the effect of K^+ and Ca^{+2} ion channel activities on the impedance signal in the presence and absence of ion channel blockers. The tight fit of a single cell to the measurement electrodes ensured reduction of the extracellular shunt current, and therefore, the effect of the cell on the impedance signal became more pronounced. One other study measured impedance of single cells on chemically modified gold electrodes that are specifically fabricated to facilitate single cell adhesion on them (Thein et al., 2010). Furthermore, instead of utilization of electrode pairs to measure bulk impedance of single cells, several electrodes can be placed around the cell, for example, in order to map the cell membrane capacitance of a single cell. Dharia et al. (Dharia et al., 2009) measured the spatial distribution of membrane capacitance of *Xenopus* oocytes by utilizing the measurements from 8 electrodes around the cell. Additionally, electrochemical impedance microscopy was coined by Wang et al. (Wang et al., 2011), where in contrast to conventional impedance spectroscopy, no micro-electrodes are needed, and submicron resolution of local impedance is possible. One futuristic approach

in single cell measurements would be the utilization of biologically inert nano-electrodes to obtain electrochemical signals inside the cell, perhaps to identify single molecule events.

1.1.1.1 Microfabrication of Microfluidic Devices

Microfluidic devices can be divided into two main units based on material and fabrication aspects: 1) Body; 2) Electrodes. Perhaps the two most important considerations for material selection and microfabrication of such microfluidic devices are material functionability and manufacturability. Electrodes usually function to modify electromagnetic fields, to detect or supply electric signal into the domain. Channels, chambers, and pillars that constitute a microfluidic device's body are usually manufactured in the sub-millimeter range, and usually they are employed to convey the fluid, to hold the fluid or the particles in the fluid. Other aspects, such as biocompability, mechanical resilience, optical transparency, or chemical resistance may play a role in material selection depending on the purpose of the device. For example, long term use of platinum black, which was found to be toxic to cells and mechanically unstable in cell culture, should be avoided. According to Lee and Sundararajan (Lee and Sundararajan, 2010) the types of materials that are available for channel and pillar micro-fabrication can be listed as: 1) PDMS (Polydimethylsiloxane), 2) Negative tone photoresists, 3) PMMA, 4) Glass, 5) Silicon, 6) Polyimides. PDMS is the most widely investigated material in microfluidics, perhaps owing to its low price. For instance, commercially available PDMS Sylgard 184 (Dow Corning) costs around $50 for 1.1 lb package, which would allow fabrication of hundreds of microfluidic devices. PDMS is a silicone based organic polymer, which has repeated methyl groups on the surface. Upon exposure to oxygen

plasma silanol groups develop on the surface of PDMS at the expense of methyl groups. As silanol groups are polar in nature, the otherwise hydrophobic surface of PDMS becomes hydrophilic, and upon contact with glass or silicon, an irreversible bond occurs through Si-O-Si bonds. Optimum plasma parameters, such as chamber pressure, duration, and plasma power have been found for strong bonding of PDMS to glass (Bhattacharya et al., 2005). PDMS can be made photopatternable by addition of photosensitive chemicals (Desai et al., 2007), which are commercially available (WL5150, Dow Corning). In addition, its mechanical properties can be enhanced by doping it with nanomaterials, such as carbon nanotubes (Dyke and Tour, 2004). PDMS can be casted to a master and peeled after it is cured. This process, to yield patterns on PDMS, is called soft-lithography. In this way, several microfluidic channels can be produced from a single master. Bonding to a substrate is generally done by rendering the PDMS surface hydrophilic after exposing it to oxygen plasma. When thinner layers of PDMS or a through hole is desired, a sacrificial photoresist layer can be utilized underneath the PDMS layer. The sacrificial photoresist layer can then be removed by lift-off techniques, leaving a patterned PDMS structure behind (Oh, 2008; Park et al., 2009). Alternatively, it can be patterned by plasma etching (Balakrisnan et al., 2009). One other application of PDMS is to build membranes or flexure components in microfluidic systems that are enabled due to hyperelastic nature PDMS (Unger et al., 2000).

The introduction of PDMS into microfluidic technology has fueled the fabrication of microdevices for particle manipulation by DEP (McDonald et al., 2000). PDMS structures have numerous advantages over the structures that are fabricated by conventional fabrication techniques, such as chemical etching. Biocompatible, robust,

thermally low conductive, and as well as ease of alignment, and being able to be processed under regular bench top laboratory conditions, made PDMS a firm building block of micro-devices for dielectrophoretic manipulation of biological materials (Park et al., 2011; Lewpiriyawong et al., 2010; Kanagasabapathi et al., 2005).

Photolithography is another technique for patterning materials to build microfluidic channels, chambers, and pillars. Basically, in photolithography a spin coated polymer is selectively cured by UV light. The cured part can then become soluble or insoluble to a developer depending on the tone of the photoresist (positive or negative). A pattern is then obtained by developing the UV light treated coat in a solvent. Negative tone photoresists, such as SU-8, are generally used to fabricate structures for microfluidic systems. SU-8 is an epoxy-based photocurable resin that can be processed to have high aspect ratio, and it is widely used in microfluidic systems (commercially available from MicroChem Corporation). Microfluidic structures or masters for soft-lithography can be obtained by photo-patterning SU-8; however, the epoxy based nature of SU-8 makes it incompatible with long term studies of cells. Nevertheless, SU-8 can be rendered hydrophilic and biocompatible by modifying the surface with HNO_3-ceric ammonium nitrate (HNO3-CAN) and ethanolamine (Stangegaard et al., 2006). In addition, SU-8 has an electroosmotic flow performance similar to that of glass (Sikanen et al., 2005). Polymethylmethadrylate (PMMA) is another material that is used to build microfluidic structures. PMMA is an optically transparent thermoplastic material that can be patterned by fast fabrication methods such as hot embossing (Lee and Sundararajan, 2010). On the other hand, PDMS is a thermoset material that requires longer curing times compared to PMMA. Silicon and glass are two other types of materials, which are mainly used where

stiffness is required. For instance, for acoustophoretic manipulation of particles polymeric structures cannot be used; instead, rigid materials such as glass and silicon are preferred (Koklu et al., 2010). While glass can be etched isotropically by concentrated hydrofluoric acid, wet etching of silicon is highly dependent on the orientation of its crystal plane. Both silicon and glass are commonly used as substrates to hold the microfluidic structures.

The deposition methods of electrode materials can be physical or chemical in nature. In physical vapor deposition a source metal is raised to high energy and targeted to the substrate. Evaporation, sputtering, and pulsed laser deposition are common ways to deposit metals on substrates. In evaporation a target material is vaporized by delivering energy either by electron beams, resistive or inductive heating. The success of evaporation of different materials is based on the temperature that can be achieved in the chamber. Elements that have higher melting points like tungsten ($3370^{o}C$) are much more difficult to evaporate. In sputtering a target material is placed in a chamber that has plasma, and the target is lifted by ion bombardment. Usually the thickness of the deposited layer cannot be greater than 1 μm, which would take 1 hour to complete by sputter coating. A physical obstruction or a sacrificial layer can be utilized to pattern the deposited metal layer. A pattern of photoresist material underneath the deposited layer can serve as a sacrificial layer. The deposited layer can then be patterned by lifting off the photoresist in a solvent. Electroplating is a chemical way to achieve metal deposition with thickness much greater than that which can be achieved by physical vapor deposition. Electroplating includes transfer of metal atoms in one electrode into another in an electrolyte under DC bias. Electroplating usually requires a seed layer, which can be

deposited by sputtering, to grow a metal on it. Thick photoresist layers can alternatively serve as a mask for determining the boundaries of the electroplated metal. By electroplating one can achieve a film thickness of several hundreds of microns. More recently, an AFM (atomic force microscopy) tip can be utilized to deliver conductive material onto a surface. This process is called dip-pen nanolithography. The line width obtained by this method can be as small as a few tens of nanometers. Old Dominion University Biomicrofluidics laboratory has such a device.

The most commonly used electrode materials are gold and platinum, mainly due to their resistance to corrosion and oxidation. Although copper is a better conductor than gold and platinum, it is not widely preferred because of its slow oxidation by atmospheric oxygen. Both platinum and gold electrodes suffer from electrode polarization at the interface when used as electrodes. The low surface roughness of gold and platinum electrodes lessens the effective surface area, and thereby the double layer capacitance. Usually electrode polarization is dominant in the low frequency range (~10 kHz), and masks the recorded signal. One way to avoid electrode polarization is to roughen the electrode surface either by sandblasting or by using electrochemical treatments to cover the electrode surface with a fractal or porous material. The most common way to electrochemically modify the surface is platinum black (PB) treatment; as a historical note Fricke (Fricke and Morse, 1925) used PB electrodes to suppress electrode polarization when he measured red blood cell impedance. Recently, performances of titanium nitride (TiN), iridium oxide (IrOx), and polypyrrole/polystyrenesulfonate (PPy/PSs) electrodes have been evaluated (Malleo et al. 2010). Among them PPy/PPs electrodes were found to have 800 folds larger double layer capacitance when compared

to bare platinum electrodes. The PPy/PPs electrodes were evaluated to have a stable structure if they were stored wet over a period of 10 days. No toxic effects of PPy/PPs electrodes on cells have been reported.

1.2   Overview

The introduction section to this dissertation focused on both conventional and microfluidic cell impedance spectroscopy. The major dielectric spectroscopy techniques are listed and recent methods such as microfluidic dielectric spectroscopy are reviewed. Dielectrophoresis and electrorotation can also be used as single cell dielectroscopy tools, as they also depend on cell polarization. As a final word, conventional dielectric spectroscopy tools are being miniaturized by microfluidics, which will probably lead to small scale single cell dielectric spectroscopy analyzers in the future. Such technologies will enable quantification of biological processes and provide extra insight to understand the complex nature of biological cells.

CHAPTER 2

THEORY

In this section the basic theory behind particle polarization is given. First, the notion of complex permittivity is explained. The polarization of a particle that is situated in a uniform electric field is discussed. Double layer effects on particle polarization are addressed in detail. Discussion of particle polarization is extended to biological cells. Basic models to describe cell polarization are given. Chapter II ends with discussion of particle electromechanics.

2.1 Basic Dielectric Theory

2.1.1 Point Dipole in a Uniform Electric Field

Assume two equal and opposite charges ($+q, -q$) are held together by some fundamental forces in a uniform electric field (Figure 2.1). The dipole moment is defined as $\bar{p} = q \cdot \bar{d}$, where $\bar{d}$ is the vector of length d between the charges. The potential energy of the dipole is the scalar product of the electric field vector and the dipole moment, $u = -\bar{E} \cdot \bar{p}$. For θ = 0 (θ: the angle between vectors $\bar{p}$ and $\bar{E}$), the potential energy of the dipole is at minimum, whereas for θ = 180°, the potential is at maximum. As a consequence, if θ is different than zero the dipole will orient itself relative to the electric field until the angle between the dipole and the electric field becomes zero. At this point the dipole is at its minimum. The dipoles can be naturally found in the nature; water and other polar

molecules like formic acid are examples of permanent dipoles. A dipole can also be induced by the application of an electric field. A dielectric (insulating) material such as rubber can become polarized by an external field, and can *permit* the flow of electricity for alternating fields.
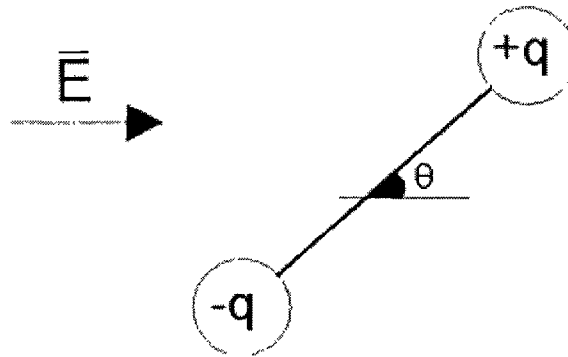
Figure 0.1 A dipole in uniform electric field

The strength of the induced dipole moment is proportional to the electric field, $\bar{p} = \alpha \bar{E}$. To a first order approximation, α is a constant, and the angle between electric field and the moment is zero. However, in general the dipole moment $\bar{p}$ is proportional to the electric field $\bar{E}$ such that $\bar{p} = \varepsilon_0 \chi \bar{E}$, where χ is the susceptibility of the material. The relative permittivity is defined as $\varepsilon = 1 + \chi$. Now an alternating electric field, which is defined by $\bar{E} = E e^{i\omega t} \hat{x}$, where $\hat{x}$ is the unit vector, is assumed to act on the dipole. In alternating fields permittivity is a complex quantity such that $\tilde{\varepsilon} = \varepsilon' - i\varepsilon''$. At low frequencies the dipole can follow the alterations of the electric field so the real part of permittivity is high, and it is equal to the static permittivity that will be referred to as ε'_s.

As the frequency approaches the relaxation frequency (τ_{rel}^{-1}), the dipole fails to follow the

alternations of the electric field, and the real part of permittivity will start to decrease consequently. At frequencies much higher than τ_{rel}^{-1} the permittivity will reach its limiting value that will be referred as ε'_{∞}. The imaginary part of the permittivity will give a peak at τ_{rel}^{-1}. The peak in the imaginary part is due to the heat that is generated during the alignment of dipole, which is acting against the randomizing effects of the Brownian motion. In other words, the real part of the permittivity is the storage part, while the imaginary part is the dissipative part of electric energy. The static conductivity of the medium also contributes to the dissipation part of the complex permittivity. The phenomenon described above is usually referred to as the dielectric relaxation, with τ_{rel}^{-1} being the relaxation frequency. For water the relaxation frequency is about $2 \cdot 10^{10}$ Hz. At frequencies lower than this, the relative permittivity of water is around 80. As the frequency increases, relative permittivity drops to about 2. The relaxation frequency of water is around the operating frequency of the microwave ovens, which is about 2 GHz. The drop in the permittivity of the material is due to the dipoles' inability to follow the field. The formation of the dipole can be by electronic, atomic, and ionic means at the atomic level as well. In electronic polarization the electron cloud around the nuclei becomes polarized; in atomic polarization disposition of nucleus causes polarization, and in ionic polarization cations and anions switch their positions. However, the mentioned atomic mechanisms occur in the high frequency range (around the terahertz range), and therefore in this study atomic effects are not considered. A sketch of a single relaxation complex permittivity is given in figure 2.2, where solid and dashed lines represent real and imaginary parts of complex permittivity, respectively.

The above theory of the dielectric relaxation can also be applied to bulk materials. The proportionality between the electric field and the electric current is defined as conductivity of the material, and in alternating fields this is a complex quantity. The electric current consists of two parts; a current due to flow of charge carriers and a current due to polarization of material, which is defined as the displacement current by Maxwell.

$$\omega / 2\pi \tau_{rel}$$
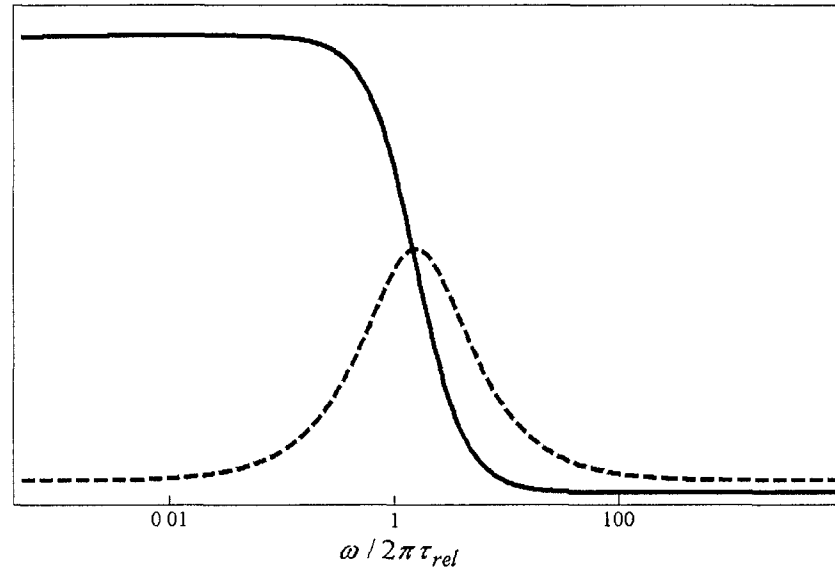
Figure 0.2 Debye type single relaxation spectra with arbitrary parameters. Solid and dashed lines represent real and imaginary parts of the permittivity

The total current through a material in an alternating field is given as $J_t = J + J'$, where the displacement current is given as

$$J' = \frac{\partial D}{\partial t}, \tag{1}$$

where D is the electric displacement, and it is connected to the electric field by $D = \varepsilon \varepsilon_0 E$. In a sinusoidal alternating field varying with angular frequency ω, we find

the complex conductivity as $\tilde{\sigma} = \sigma - i\omega\varepsilon\varepsilon_0$ through the relation $\bar{J} = \tilde{\sigma} \cdot \bar{E}$. The complex permittivity is an analog of complex conductivity, and they differ only by the factor $-i\omega$.

In order to derive a constitutive equation for permittivity, polarization of a material is assumed to be composed of two parts, $\bar{p}_1$ and $\bar{p}_2$ with corresponding χ_1 and χ_2, where $\bar{p}_2$ is assumed to undergo a relaxation process at a rate proportional to $(\chi_2 E - P_2)$. In an alternating field the solution for $\bar{p}$ is given as (Pethig, 1979):

$$\bar{p} = \bar{p}_1 + \bar{p}_2 = \left(\chi_1 + \frac{\chi_2}{1 + j\omega\tau} \right) E \tag{2}$$

This process yields the complex permittivity as

$$\tilde{\varepsilon} = \varepsilon_\infty + \frac{(\varepsilon_s - \varepsilon_\infty)}{1 + i\omega\tau_{rel}} - i\frac{\sigma}{\omega\varepsilon_0}, \tag{3}$$

where ε_s and ε_∞ are limiting low and high frequency values for permittivity, respectively, and σ is the static (DC) conductivity of the material. The real and imaginary parts of the above equation are given respectively as:

$$\varepsilon' = \varepsilon_\infty + \frac{(\varepsilon_s - \varepsilon_\infty)}{1 + \omega^2\tau_{rel}^2}, \tag{4a}$$

$$\varepsilon'' = \frac{(\varepsilon_s - \varepsilon_\infty)\omega\tau_{rel}}{1 + \omega^2\tau_{rel}^2} - i\frac{\sigma}{\omega\varepsilon_0}, \tag{4b}$$

The above equation set is known as the Debye dispersion formulas. If symmetrical distribution of relaxation times is present around the mean relaxation time, the complex permittivity can be described by the Cole-Cole equation (Pethig, 1979):

$$\widetilde{\varepsilon} = \varepsilon_\infty + \frac{(\varepsilon_s - \varepsilon_\infty)}{1 + (i\omega\tau_{rel})^\beta} - i\frac{\sigma}{\omega\varepsilon_0}, \tag{5}$$

In the above equation β converges to 1 for single dispersion; whereas it converges to 0 for a dispersion occurring in infinite time. The Davidson and Cole model describes the complex permittivity if non-uniform distribution of relaxation times is present around the mean relaxation time (Pethig, 1979):

$$\widetilde{\varepsilon} = \varepsilon_\infty + \frac{(\varepsilon_s - \varepsilon_\infty)}{(1 + i\omega\tau_{rel})^\gamma} - i\frac{\sigma}{\omega\varepsilon_0}, \tag{6}$$

where γ is a constant between 0 and 1.

In general, if there are multiple relaxation times in the material, each with a different relaxation time that is given as $\tau_1, \tau_2, \tau_3, \ldots$, then the complex permittivity takes the following form,

$$\widetilde{\varepsilon} = \varepsilon_\infty + \frac{\Delta\varepsilon_1}{1 + i\omega\tau_1} + \frac{\Delta\varepsilon_2}{1 + i\omega\tau_2} + \ldots - i\frac{\sigma}{\omega\varepsilon_0}. \tag{7}$$

In a general sense the complex permittivity is given as the following,

$$\widetilde{\varepsilon} = \varepsilon_\infty + (\varepsilon - \varepsilon_\infty)\int_0^\infty \frac{p(\tau)d\tau}{1 + i\omega\tau} - \frac{i\sigma}{\omega\varepsilon_0}, \tag{8}$$

where,

$$\int_0^\infty p(\tau)d\tau = 1.$$

Equation 8 is a general formula that can describe a material's relaxation processes provided that a suitable distribution function (p) is chosen.

2.2 Polarization of a Dielectric Sphere

2.2.1 A Dielectric Sphere in Non-ionized Media

We assume that a dielectric sphere is put in an electrolyte free (but conducting) media, and an external field is applied from the two ends of the media. In this case the electrostatic boundary condition on the surface of the sphere is given by $\varepsilon_p \overline{E}_p \hat{n} = \varepsilon_m \overline{E}_m \hat{n}$, where p and m are subscripts for particle and medium, respectively. This condition holds if the interface is free of charge. Then the ratio of particle and medium current densities at the interface will be,

$$\frac{\overline{J}_p}{\overline{J}_m} = \frac{\sigma_p \cdot \overline{E}_p \cdot \hat{n}}{\sigma_m \cdot \overline{E}_m \cdot \hat{n}} = \frac{\sigma_p \cdot \varepsilon_p}{\sigma_m \cdot \varepsilon_m}. \tag{9}$$

If this ratio is different than 1, then the interface will be charged proportional to the local current densities, and the above boundary condition for electric field will not hold anymore. The amount of charge trapped at the interfaces is proportional to the frequency of the applied field. With decreasing frequency, increased amounts of charge will be trapped at the poles (boundaries) of the particle. The particle will hold a dipole at frequencies lower than the interfacial relaxation frequency. If the frequency is increased above this frequency, the dipole will vanish and the particle will be shunted. To a

reasonable approximation the system can be considered as a capacitor and a resistor in parallel, where resistor and capacitor represent medium and dielectric particle, respectively. The relaxation time will be the RC time constant of the circuit. In other words, the time to charge the dielectric sphere through resistive medium is given as

$$\tau_\beta = \varepsilon_p / \sigma_m .$$
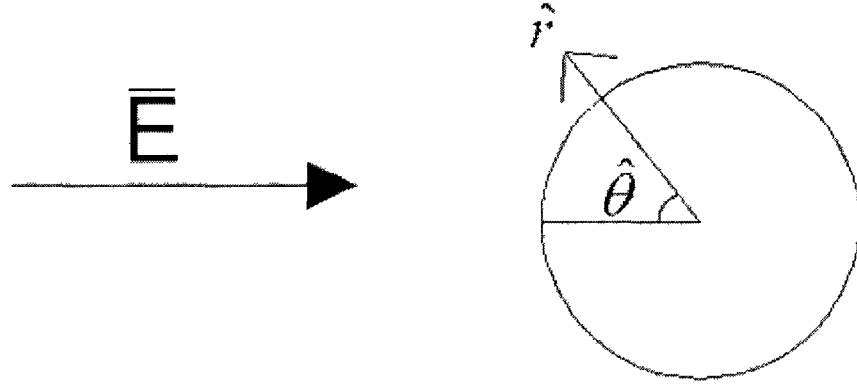
Figure 0.3 A spherical particle in uniform electric field

The potential around and inside a lossy dielectric sphere ($\varepsilon_p^* = \varepsilon_p - i\sigma_p / \omega$) in a lossy medium ($\varepsilon_m^* = \varepsilon_m - i\sigma_m / \omega$), which is schematically shown in figure 2.3, under external field $E \cdot \hat{x}$ is given by the following equations, respectively (Morgan and Green, 2003),

$$\varphi_m = Ea^3 f_{CM} \frac{\cos\theta}{r^2} - Er\cos\theta, \tag{10a}$$

$$\varphi_p = -\left(\frac{3\varepsilon_m^*}{\varepsilon_p^* + 2\varepsilon_m^*} \right) Er\cos\theta, \tag{10b}$$

where r and θ are the polar coordinates; m and p stands for medium and particle, respectively; a is the radius of particle, and f_{CM} is the Clausius-Mossotti (CM) factor given by,

$$f_{CM} = \frac{\varepsilon_p^* - \varepsilon_m^*}{\varepsilon_p^* + 2\varepsilon_m^*}.$$ (11)

The first term in equation 10a is due to the presence of the particle, whereas the second term is due to the external electric field. By equating the first term in equation 10a to the potential of a point dipole, the dipole moment of the particle is found as,

$$\overline{p} = 4\pi\varepsilon_m f_{CM} a^3 \overline{E}.$$ (12)

The dipole moment of the particle may lie parallel or anti-parallel to the electric field depending on the polarizability of the particle. The relaxation due to such effects is usually termed the Maxwell-Wagner or interfacial relaxation. The relaxation time of such a system is usually called the Maxwell-Wagner relaxation frequency and is given as,

$$\tau_\beta = \frac{\varepsilon_p + 2\varepsilon_m}{\sigma_p + 2\sigma_m}.$$ (13)

Equation 11 describes the effective polarizability of a homogenous solid spherical particle in an otherwise uniform electric field; however, as the particle is modified to include a shell or different relaxation mechanisms are thought to play a role in the particle polarizability, the algebraic calculation and the representation of equation 11 becomes complex. Therefore, it will be convenient to express the CM factor as a sum of

the relaxation processes. The formulation of the generalized CM factor is given by (Jones, 1995),

$$f_{CM} = f_{CM}^{\infty} - \frac{\Delta f_{CM}^{\alpha}}{i\omega\tau_{\alpha}+1} - \frac{\Delta f_{CM}^{\beta}}{i\omega\tau_{\beta}+1} - \cdots - \frac{\Delta f_{CM}^{N}}{i\omega\tau_{N}+1},$$ (14)

where $\tau_{\alpha}, \tau_{\beta}, ..., \tau_{N}$ are the relaxation times of the system of interest, f_{CM}^{∞} is the limiting CM factor, and Δf_{CM}^{N} is the CM factor increment of the Nth relaxation. For instance, a spherical particle with a thin shell will experience two relaxation times as there are two interfaces in the system. For a homogenous lossy dielectric sphere equation 14 becomes,

$$f_{CM} = f_{CM}^{\infty} + \frac{f_{CM}^{0} - f_{CM}^{\infty}}{i\omega\tau_{\beta}+1},$$ (15)

where,

$$f_{CM}^{\infty} = \frac{\varepsilon_p - \varepsilon_m}{\varepsilon_p + 2\varepsilon_m},$$

$$f_{CM}^{0} = \frac{\sigma_p - \sigma_m}{\sigma_p + 2\sigma_m}.$$

2.2.2   Dielectric Spheres in Non-ionized Media

Maxwell was the first to calculate the conductivity of a sphere that is bearing smaller spherical particles with volume fraction p. Formulation for the suspension conductivity (σ_{sus}) according to this approach is given as,

$$\frac{\sigma_{sus} - \sigma_m}{\sigma_{sus} + 2\sigma_m} = p\frac{\sigma_p - \sigma_m}{\sigma_p + 2\sigma_m}. \tag{16}$$

The main assumption in Maxwell's theory was that the electrical interactions between the particles is negligible, which in turn requires small values of p. Later, Wagner extended Maxwell's theory to alternating currents, where he also assumed low values of p. Equation 16 reduces to a simple mixture formula with no dispersion, when terms with second and higher powers of p are neglected and $\sigma_p \ll \sigma_m$ is assumed. In this case, however, inclusion of complex parameters (Wagner's model) predicts a small dispersion that is equivalent to the charging (RC) time constant of the medium. A large dispersion in the Maxwell-Wagner mixture model requires particle properties (σ_p and ε_p) to be much larger than those of the medium.

A more general extension of the Maxwell mixture model is that of Fricke's, which is given as (Fricke, 1924),

$$\frac{\sigma_{sus}^* - \sigma_m^*}{\sigma_{sus}^* + \lambda\sigma_m^*} = p\frac{\sigma_p^* - \sigma_m^*}{\sigma_p^* + \lambda\sigma_m^*}, \tag{17}$$

where λ is the shape factor, which takes a value of 2 for spheres and 1 for cylindrical particles oriented normal to the field, and σ^* refers to complex permittivity.

The complex permittivity of the mixture for spherical particles suspended in a medium is derived elegantly in the textbook by Jones (Jones, 1995). According to this approach suspension complex permittivity can be written in terms of the CM factor,

$$\varepsilon^*_{sus} = \varepsilon^*_m \frac{1 + 2pf_{cm}(\varepsilon^*_p, \varepsilon^*_m)}{1 - pf_{cm}(\varepsilon^*_p, \varepsilon^*_m)}, \tag{18}$$

where linear superposition of dipole moments of spheres is used in the derivation. This approach also neglects the particle interactions.

As discussed before, Maxwell-Wagner mixture theory is correct for dilute suspensions of particles, while at higher concentrations interparticle interactions come into play. The externally applied electric field generates an electroosmotic flow around the particle by dragging the counterions along the particle surface. Electroosmotic flow around the particle resembles Stokes' first problem in fluid mechanics, where the fluid in the double layer moves with a terminal velocity and the shear is dissipated by the medium viscosity. In a particle suspension it can be assumed that the flow is steady and there are no external pressure gradients. In this case flow is governed by the Laplace equation, and it resembles potential flow. The velocity field around the particle decays with $1/r$, where r is the distance from the particle. The electric field of a dipole decays with $1/r^3$ that is faster than the hydrodynamic field. The hydrodynamic field should be considered when accounting for large volume fractions; however, such a correction has never been attempted.

For concentrated suspensions of particles, the Maxwell-Wagner mixture formula should be corrected for particle interactions. The Hanai-Bruggemann theory extends the Maxwell-Wagner mixture model for high particle concentration (Hanai, 1968),

$$\left[\frac{\varepsilon^*_{sus} - \varepsilon^*_p}{\varepsilon^*_m - \varepsilon^*_p} \right]\left[\frac{\varepsilon^*_m}{\varepsilon^*_{sus}} \right]^{1/3} = 1 - p. \qquad (19)$$

If the particle complex permittivity is larger than that of the medium, the particle interactions become more dominant, which means Maxwell-Wagner mixture theory is more accurate for biological cells in the low frequency region because of the non-conducting cell membrane. A more rigorous approach would be to expand the suspension complex permittivity to the nth order in p by considering the hydrodynamic interactions.

2.2.3   Dielectric Sphere in Ionized Medium

When a particle is immersed in an ionic environment, an ionic structure occurs around the surface. This structure is called the electric double layer. Generation of the double layer depends on the surface charge and the ionic species. Usually generation of the surface charge is of non-electrostatic origins; it can either depend on the specific adsorption of an ion to the surface, adsorption of an anionic surfactant, or pH of the surrounding electrolyte (Of course on the atomic level all these interactions are of electromagnetic origin). The extent of the double layer is determined by the competition between diffusion and electrostatic forces. As a result, the particle surface charge is screened by the counter-ions in the surrounding double layer. The double layer consists of two parts: diffuse and Stern layers. In the Stern layer, ions are bound to the surface, and usually it is one or two ion diameters thick. The plane at the outer extent of the Stern layer is referred to as outer Helmholtz plane, and if specific adsorption is present in the system, the plane that bears the specifically adsorbed ions is called the inner Helmholtz plane. Also, about a couple of molecular distances away from the surface, there exists a

hydrodynamic slip plane. Below this hydrodynamic slip plane ions are bounded to the surface, and hydrodynamic forces cannot ordinarily move them. The potential at this plane is called ζ or the electrokinetic potential. A schematic diagram of a double layer is shown in figure 2.4.

The ions in the diffuse layer obey the Boltzman distribution:

$$n_i(x) = n_o\, e^{-\frac{z_i e\, \psi(x)}{kT}}, \tag{20}$$

where n_o is the bulk concentration of ion species i, ψ is the electric potential, e is the electronic charge, T is the temperature, and z_i is the valency of species i. The potential distribution in the diffuse layer is governed by the Poisson equation, and the combination of equation 20 and the Poisson equation for the electric field yields the Poisson Boltzman (PB) equation. Assuming a symmetrical electrolyte in valence the PB equation in non-dimensional form becomes,

$$\frac{d^2(z\Psi)}{d(\kappa x)^2} = \sinh(z\Psi), \tag{21}$$

where

$$\Psi = \frac{e\psi}{kT},$$

and

$$\kappa^2 = \frac{2e^2 n_0 z^2}{\varepsilon kT}.$$

The parameter κ^{-1} in the above equations is a measure of the double layer thickness. For a flat plate the solution for the electric field in the diffuse layer becomes (Gouy Chapman theory)

$$E(x) = \sqrt{\frac{8 n_o kT}{\varepsilon}} \sinh\left(\frac{ze\,\psi(x)}{2kT}\right).$$ (22)

Extensive analysis of double layer and specific adsorption can be found in the textbooks by Lyklema (Lyklema, 1995), Hunter (Hunter, 2001), and Israelachvili (Israelachvili, 2011). Having surface charge at one end and volume charge distributed over the double layer, electrically double layer behaves as a lossy capacitor. Empirically double layer impedance is in the form of constant phase angle impedance,

$$Z_{dl} = \frac{\alpha}{(i\omega)^{\beta}}.$$ (23)

In the above equation α and β are constants, and ω is the angular frequency of the applied field. More specifically the double layer can be treated as a series combination of Stern and double layers impedances. The capacitance of the diffuse layer, when the volume charge distribution is neglected, can be approximated as,

$$C_d = \varepsilon\kappa\, A.$$ (24)

The above formulation is equal to the value of a parallel plate capacitor that is filled with material of dielectric permittivity ε with thickness κ^{-1} over area A. Usually the impedance of the double layer on the test electrodes annihilates the potential applied to liquid systems; therefore, even though it cannot be totally prevented, its effect should be

lessened (Malleo et al., 2010b) or should be ruled out (Bordi et al., 2001). One way to lessen the effect of double layer is to increase the effective electrode area by using porous electrode coatings, such as platinum black.

Ions in the salt solutions are subject to various mechanical forces such as Brownian motion (diffusion), conduction, and hydrodynamic forces. The ionic current of species i is given by the Nernst-Planck equation,

$$\bar{J}_i = -D_i \bar{\nabla} c_i - \frac{z_i}{|z_i|} c_i u_i \bar{\nabla} \psi + c_i \bar{\upsilon}, \tag{25}$$
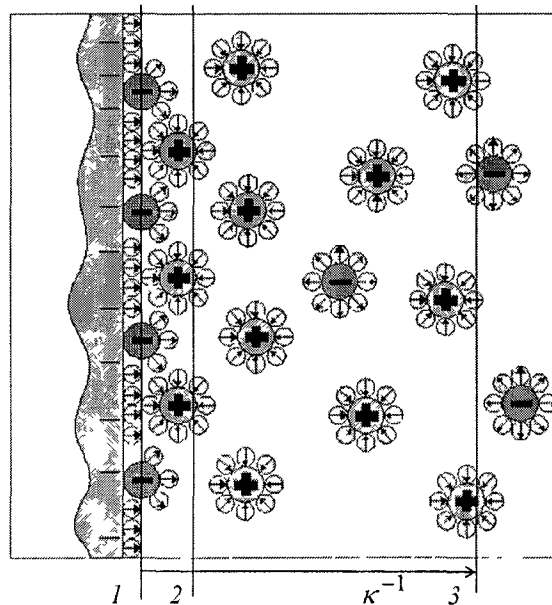
Figure 0.4 A schematic view of an electrical double layer. A single layer of cations forms the Stern layer on a negatively charged surface of adsorbed anions. The extent of Debye length is shown by κ^{-1}. Layers 1, 2, and 3 correspond to inner and outer Helmtoltz planes and extent of electrical double layer, respectively

where u_i is the mobility of species i, and $\bar{\upsilon}$ is the velocity vector of hydrodynamic flow. For an incompressible fluid the ionic transport equation is,

$$\frac{\partial c_i}{\partial t} = -\overline{\nabla}.\overline{J}_i = D_i \nabla^2 c_i + \frac{z_i}{|z_i|} u_i \overline{\nabla}.\left(c_i \overline{\nabla} \psi\right) - \overline{\upsilon}.\overline{\nabla} c_i. \tag{26}$$

In the derivation of the Maxwell-Wagner interfacial dispersion, the electric fluxes were assumed to be occurring through the surface, not around the surface; however, in real systems current can also flow either around or through the particle due to the presence of conducting double layer or surface charge layers. The inclusion of the double layer will alter the derivation given above. Conservation of electric charge on the particle boundary will be altered by the inclusion of surface conductivity, where subscript y denotes surface component (Jones, 1995),

$$J_{\perp m} - J_{\perp p} + \frac{\partial \sigma_f}{\partial t} + \nabla_y \cdot \overline{J}_y^* = 0, \tag{27}$$

where

$$\sigma_f = \varepsilon_m E_{\perp m} - \varepsilon_p E_{\perp p}.$$

In the above equations σ_f is the free charge generated by the imbalance of fluxes, the subscript $\perp$ denotes the normal component, and $\overline{J}_y^*$ is the complex surface current density defined as,

$$\overline{J}_y^* = i\omega \varepsilon_y^* \overline{E}_{\tan}, \tag{28}$$

where ε_y^* is the complex permittivity of the double layer (or mobile surface charge groups) and subscript tan denotes tangential component. The complex currents around a

particle are schematically shown in figure 2.5. Solution for the potential around the particle yields a correction to the particle complex permittivity,

$$\varepsilon_p^{*'} = \varepsilon_p^* + 2\frac{\varepsilon_y^*}{a}. \qquad (29)$$

However, surface conductance cannot be solely attributed to the conduction in the double layer, as absorbed ions or mobile proteins can also move around a particle or a cell and the membrane itself is a 2 dimensional fluid. These effects are omitted in this dissertation. The same analysis was also published by O'Konski (O'Konski, 1960), where he also derived complex permittivity increments due to surface conductance. The surface conductance effect is more dominant for particles less than 1 μm in diameter as there is $1/r$ dependence. As a consequence interfacial relaxation of viruses, protein and nanoparticle suspensions are strongly influenced by surface conductance. For more information, we refer to the previous investigations that are performed on various particles including nanoparticles (Froude et al., 2010; Green and Morgan, 1998; Zhao and Bau, 2010).
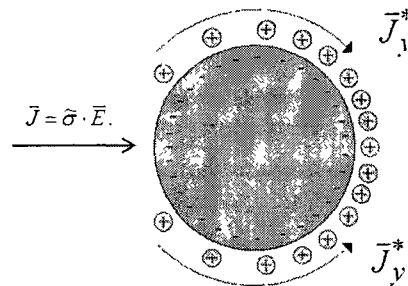
Figure 0.5 Complex tangential current $\overline{J}_y^*$ around a representative particle.

Additional effects on interfacial polarization have to be considered for electrical double layers. When a particle is put in an ionized medium and an electric field is set as shown

in figure 2.5, the ions in and around the double layer will be set in motion due to diffusion, conduction, and electro-osmotic flow occurring around the particle. It takes a finite time for the double layer to reorganize and form a dipole around the particle after an applied electric field; the time scale associated with this mechanism is τ_α that is $O(a^2 / D)$, where D is the ionic diffusion coefficient. A double layer becomes polarized under a stationary electric field, which means an excess charge is accumulated on one pole of the particle, leaving a depleted region on the other pole. At this instant a large dipole that has a size on the order of a is generated. This phenomenon is termed as double layer polarization or α polarization in the biophysics field.
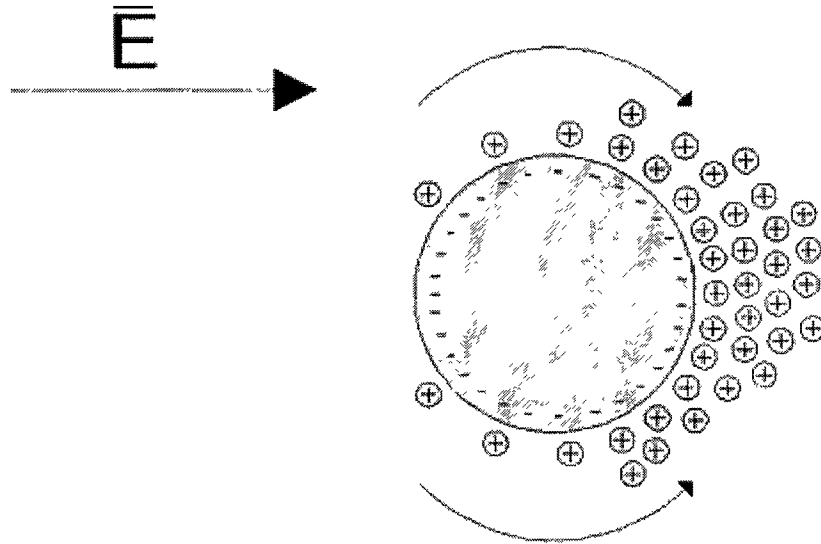
Figure 0.6 Polarization of a spherical particle's double layer in a uniform electric field. The presence of anions in the double layer is neglected

We define an important parameter in double layer polarization that describes the contribution of the surface conductance to bulk particle conductivity, namely the Dukhin number (Lyklema, 1995),

$$Du = \sigma_s / a\sigma_m.$$ (30)

The Dukhin number is the ratio of the surface conductance of a spherical particle $(2\pi a\sigma_s)$ to the conductivity of the sphere as if it had the same conductivity as the medium $(\pi a^2\sigma_m)$. If $Du \gg 1$ the electric current is shunted through the double layer; while the surface conductance becomes negligible as $Du \to 0$. In order to include the effects of Stern layer, the Du number can be re-expressed as (Lyklema, 2001),

$$Du = Du^d + Du^i,$$ (31)

where subscripts d and i stand for the diffuse and Stern layers, respectively. For a symmetric electrolyte of equal ionic diffusion coefficient, the diffuse component of Du can be expressed as,

$$Du^d = \exp\left(\frac{ze\zeta}{2kT}\right)\left(1 + 3\frac{m}{z^2}\right)\left(\frac{1}{\kappa a}\right).$$ (32)

The term m in the preceding equation is a dimensionless parameter describing the relative contribution of electroosmosis to surface conductance. The Du number for the Stern layer containing only ionic species i (counter-ions) is given as,

$$Du^i = \frac{\sigma_i^i u_i^i}{a\sigma_m},$$ (33)

where u^i is the ionic mobility and σ^i is the charge density in the Stern layer. In this part of the double layer no electro-osmosis can occur as the charges are stagnant.

When a dielectric particle with a double layer around it is put in an electric field, the polarization physics explained in the previous sections becomes more complicated as charge carriers (ions in this case) maintain their equilibrium position by means of diffusion, conduction, and hydrodynamic flow (electroosmosis). Ions in the double layer rearrange themselves when an electric field, as shown in figure 2.6, is applied. As a result of this rearrangement there is excess of one ion type at one pole and depletion of that ion type on the other pole. This is schematically illustrated in figure 2.6, where it is assumed that the surface charge on the particle cannot respond to the external electric field and the particle has very low permittivity. According to the scenario depicted in figure 2.6, we can talk about two main currents in the system (assuming current is carried by counter-ions): one is in the double layer (near field) that is due to the conduction in the double layer by counter-ions, and the other (far field) around the particle by the unbounded ions away from the particle. Also, the fluid dragged by the moving counter-ions generates a hydrodynamic flow in the double layer, dragging the co-ions. There are two ionic diffusion mechanisms corresponding to these conduction mechanisms; consequently, a steady state is reached after competition between conduction and diffusion mechanisms. At the steady state net current flowing through a unit volume is zero (no continued charge accumulation). As different length scales are involved in the processes, near and far field polarization have different relaxation times. In the near field, after double layer ions re-arrange themselves according to the external field, diffusion flux occurs normal to the particle surface. This happens because the movement of the double layer ions by conduction generates a concentration gradient relative to the neutral electrolyte (figure 2.6). The relaxation time of the motion will be on the order of $(\kappa^2 D)^{-1}$, and for typical

values of electrolytes, it corresponds to the MHz range. For the moment, this relaxation time is denoted as $\tau_{\alpha'}$. The increased concentration of counter-ions and hydrodynamically dragged co-ions at the right hand side of the particle in turn generates excess electroneutral electrolyte by diffusion and generates a depleted zone on the left hand side. Different concentrations on both poles of the particles induce an asymmetrical double layer, and consequently a dipole forms around the particle. This mechanism of polarization is the transport of the electroneutral electrolyte beyond the double layer and the relaxation time associated with this motion is on the order of $(D/a^2)^{-1}$, which is the time needed to travel around the particle (usually at kHz range), which will be denoted as τ_α. The far field relaxation is referred as α polarization or as low frequency dispersion in colloidal science.

Indeed, near field polarization and interfacial polarization can be treated in the same frames. If the particle of interest has a finite conductivity and permittivity the current into the particle will contribute to the polarization. Despite the complexity of the situation described in the preceding paragraph, the ratio of the diffusion to conduction currents in a double layer was previously shown to be on the order of $(\kappa a)^{-2}$ by O'Brien (O'Brien, 1986). Therefore, for thin double layers $(\kappa a \gg 1)$ the double layer can be treated as a thin conductive shell around the particle. Also in the same work (O'Brien, 1986) it was shown by an order of magnitude analysis that the jump across the double layer is $O(E/\kappa)$, which is negligible compared to the potential difference across particles rear and front, scales as $O(Ea)$. Thus the potential can be taken as continuous across the

double layer, and Laplace's equation needs to be solved for the electric field subject to the following boundary condition,

$$\left(i\omega\varepsilon_m + \sigma_m\right)\frac{\partial\psi_m}{\partial n} - \left(i\omega\varepsilon_p + \sigma_p\right)\frac{\partial\psi_p}{\partial n} = -\sigma_{dl}\nabla_t^2\psi_m,$$

(34)

where ∇_t is the component tangential to the particle surface. This approach will yield the same particle polarizability as in equation 29 and this can be utilized in the generalized Maxwell-Wagner mixture model (equation 18) to obtain the complex permittivity of the solution. From now on we assume that interfacial polarization and high frequency double layer polarization are both described by the above theory. Near field double layer polarization can be thought of as an extension to the interfacial polarization. This dispersion is generally referred to as δ dispersion or Maxwell-Wagner-O'Konski relaxation. Surface conductivity can be related to the ζ potential by the Du number. ζ potential is a measurable quantity using standard apparatus such as electrophoretic light scattering.

In order to derive expressions for the low frequency dispersion of colloids that is due to ionic distributions beyond the double layer, first order perturbations in Nernst-Planck and Poisson's equations were assumed (Lyklema, 1995). According to this approach application of an external field causes double layer deformation and in turn ionic diffusion; together they induce $\delta\psi$ and δc. These parameters need to be solved in the far field (from the slip plane to region beyond the double layer). In the far field (that is denoted by ff) the Nernst-Planck and Poisson equations for a symmetrical electrolyte of equal ionic diffusivities reduce to,

$$\frac{\partial \delta c^{ff}}{\partial t} = D\nabla^2 \delta c^{ff} \qquad (35)$$

and

$$\nabla^2 \delta \psi^{ff} = 0. \qquad (36)$$

In the outer boundary they are subject to the following boundary conditions,

$$\delta c^{ff} (r \to \infty) = 0$$

and

$$\delta \psi^{ff} (r \to \infty) = -E(t)r.$$

For the inner boundary conditions, ionic fluxes at the slip plane are considered. With the assumption of local equilibrium in the chemical potential and assuming the current is mainly carried by counterions (that of co-ions is negligible), the potential and ionic concentration of the far field at this boundary is given by,

$$2Du^d a\nabla_t^2 \left[-\frac{ze}{kT}\delta\psi^{ff} + \frac{\delta c^{ff}}{c_0} \right]_{surf} + \frac{\partial}{\partial r}\left[-\frac{ze}{kT}\delta\psi^{ff} + \frac{\delta c^{ff}}{c_0} \right]_{surf} = 0, \qquad (37)$$

where c_0 is the equilibrium ionic concentration in the far field. With the above information the first order electric field and ionic concentration can be solved and polarization of a single double layer can be obtained. In order to calculate complex permittivity, particles polarizability is linked to bulk values through $\tilde{\sigma} = \tilde{\sigma}_m + 3\varphi\, \hat{d}_e(\sigma_m - i\omega\varepsilon_m)$, where $\hat{d}_e$ is the dipole coefficient that is expressed by the

above quantities. The conductivity and permittivity increment is given respectively by (Lyklema, 1995),

$$\frac{\delta\sigma}{\sigma_m} = \frac{9}{8}\varphi\left(\frac{2Du^d}{1+2Du^d}\right)^2 \frac{\omega\tau\sqrt{\omega\tau}}{(1+\omega\tau)(1+\sqrt{\omega\tau}) - Du(\omega\tau)^{3/2}/(1+2Du)}, \qquad (38a)$$

$$\frac{\delta\varepsilon}{\varepsilon_m} = \frac{9}{16}\varphi(\kappa a)^2\left(\frac{2Du^d}{1+2Du^d}\right)^2 \frac{1}{(1+\omega\tau)(1+\sqrt{\omega\tau})}, \qquad (38b)$$

where $\tau = a^2/(2D)$ is the relaxation time associated with the double layer polarization. Equations 38 a and b predict a decrease in the permittivity and increase in the conductivity in the suspension at the field frequencies around the inverse of the relaxation time (τ^{-1}). In the low frequency limit the double layer can respond to the applied field and currents around the particle oppose ionic conduction, thereby reducing the suspension conductivity. At the high frequency limit the dipole around the double layer cannot form and ions can move freely around the particle; this in turn decreases the energy storing capacity of the suspension (low permittivity) and increases the dissipation in the suspension (high conduction). This process is generally referred to as α dispersion or low frequency dielectric dispersion. The generalization of this theory to arbitrary binary electrolytes and conduction behind the slip plane is given by Minor et al. (1998). The same theory was utilized to obtain the surface charge of gram positive bacteria by probing low frequency dielectric dispersion (van der Wal et al., 1997). A recent review on dielectric dispersion in aqueous colloidal systems reviews the recent progress on colloidal polarization, and reports the advances in measurement techniques as well (Grosse and Delgado, 2010).

2.3 Polarization of Biological Cells

Biological cells are often composed of a lipid-protein membrane and complex internal structure consisting of a conducting aqueous cytoplasm, organelles, cytoskeleton, and nucleus. The cell membrane consists of a lipid bilayer, which is semi-permeable. Electrically, the cell membrane is best described by a capacitor and resistor connected in parallel. A typical value for the capacitance of a cell membrane is ~1 $\mu F/cm^2$ and a typical value for its thickness is 10 *nm* (Jones, 1995). A cell membrane is selective to ion transport, and is therefore not a good conductor; however, when the cell programs itself for death (apoptosis) or it is induced by force (necrosis), the cell membrane may become leaky to ions and conductive (Pethig and Talary, 2007).

A simple single shell model can represent prokaryotic cells, which have no nucleus, and one specific eukaryotic cell: red blood cells in mammals. The complex permittivity of the cell is given as,

$$\varepsilon_c^* = \varepsilon_m^* \frac{\gamma^3 + 2\left(\dfrac{\varepsilon_{cyt}^* - \varepsilon_{mem}^*}{\varepsilon_{cyt}^* + 2\varepsilon_{mem}^*}\right)}{\gamma^3 - \left(\dfrac{\varepsilon_{cyt}^* - \varepsilon_{mem}^*}{\varepsilon_{cyt}^* + 2\varepsilon_{mem}^*}\right)},$$ (39)

where *mem* and *cyt* are indices for membrane and cytoplasm, respectively. The factor γ is given as, $\gamma = a/(a-t)$, where t is the membrane thickness. The model stems from the Maxwell-Wagner interfacial polarization theory, and therefore, two distinct dispersions will be present in the spectrum as there are two interfaces in the model. The extra dispersion caused by the presence of the cell membrane is usually termed β dispersion in

biophysics. Clausius Mossotti factors for an arbitrary cell are plotted in figure 2.7 (a) and (b), where the changes in CM due to membrane capacitance (figure 2.7a) and thickness (figure 2.7b) are also plotted. Changes in the membrane capacitance and thickness affect the crossover frequency of the first dispersion. Changes in the membrane capacitance have been connected to the cell surface morphologies, for example, membrane microvillus, blebs, folds, and ruffles (Yang et al., 1999; Pethig et al., 2002). Cells with richer surface morphologies were shown to have higher membrane capacitance than that of cells with smoother cell surfaces. As a consequence, rougher cell membranes require longer times to be charged. Also, this effect leads to smaller crossover frequencies (which is the frequency at which the CM value is zero), a behavior consistent with figure 2.7(b). This statement has led to the characterization (Pethig and Talary, 2007) and separation (Gascoyne et al., 1997) of cells with dielectrophoresis, which will be covered in detail section 2.1.5.

In the context of electromechanical manipulation and dielectric spectroscopy, the single shell model is shown to be applicable to eukaryotic cells, which hold a nucleus, in the frequency range below and about the interfacial relaxation frequency (Gascoyne et al., 1997, Foster and Schwan, 1989). A more detailed approach for eukaryotic cells is the double shell model, where the nucleus is incorporated in the model. The model can be extended to an infinitely many shelled particle, as shown previously by a smearing out technique (Huang et al., 1999). An impedance expression for a suspension with cells can be obtained by using Maxwell-Wagner mixture theory (equation 18) and replacing the particle permittivity with that of a cell (equation 39).
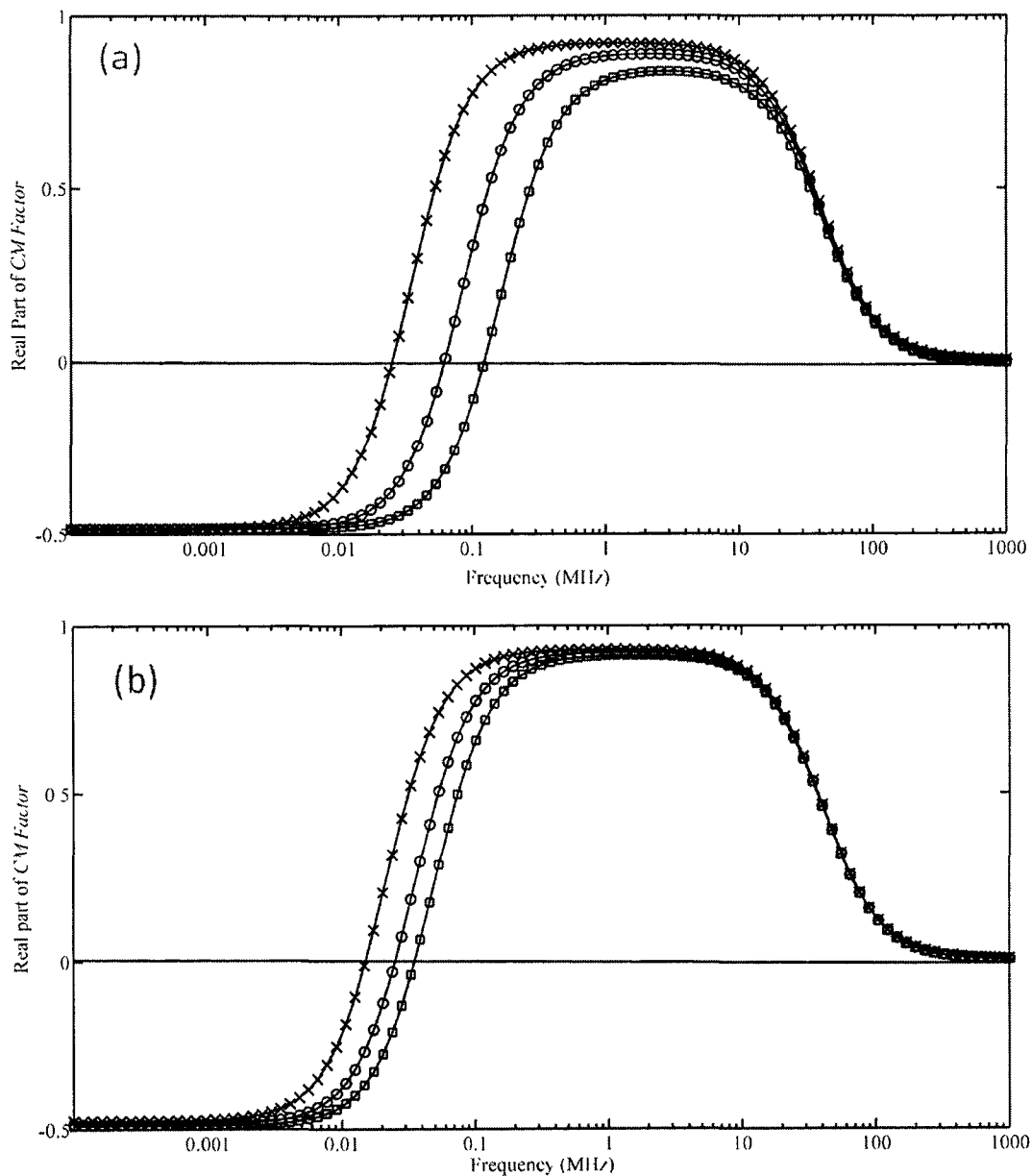
Figure 0.7 Real part of the Clausius-Mossotti factor of an arbitrary cell as a function of

the membrane capacitance (a) 8.8 $\mu F/cm^2$ (x), 3.5 $\mu F/cm^2$ (o), 1.8 $\mu F/cm^2$ ($\square$) and

membrane thickness (b) 3 nm (x), 5 nm (o), 7 nm ($\square$) in a medium of conductivity 0.01

S/m

The resulting expression is complicated to express; however, under some assumptions simple expressions can be obtained (Foster and Schwan, 1989). In figure 2.8, an arbitrary CM factor is plotted against frequency to express parameters that dominate the effective polarizability. At the range between 1 Hz and 10 MHz, in general, two dispersion mechanisms may occur, which are α and β dispersions. Although it is not possible to acquire a fine detailed picture of the cell in this frequency range as fields cannot penetrate into the cell, information about the double layer, surface charge groups, and membrane of the cells is accessible.

Figure 0.8 A representative CM factor. Dominant parameters on the CM factor at different frequency ranges are shown on the graph

Biological membranes in general are complex peripheries that perform specialized functions, such as ionic transport or insulation. Biological membranes, which are mainly composed of lipid and protein, can be classified into five main types (Pethig, 1979): 1)

Plasma, 2) Chloroplast thylakoid, 3) Mitochondrial inner cristae, 4) Retinal rods, 5) Nerve axon myelin. These membranes are composed of 50% lipid and 50% protein, except for myelin, which has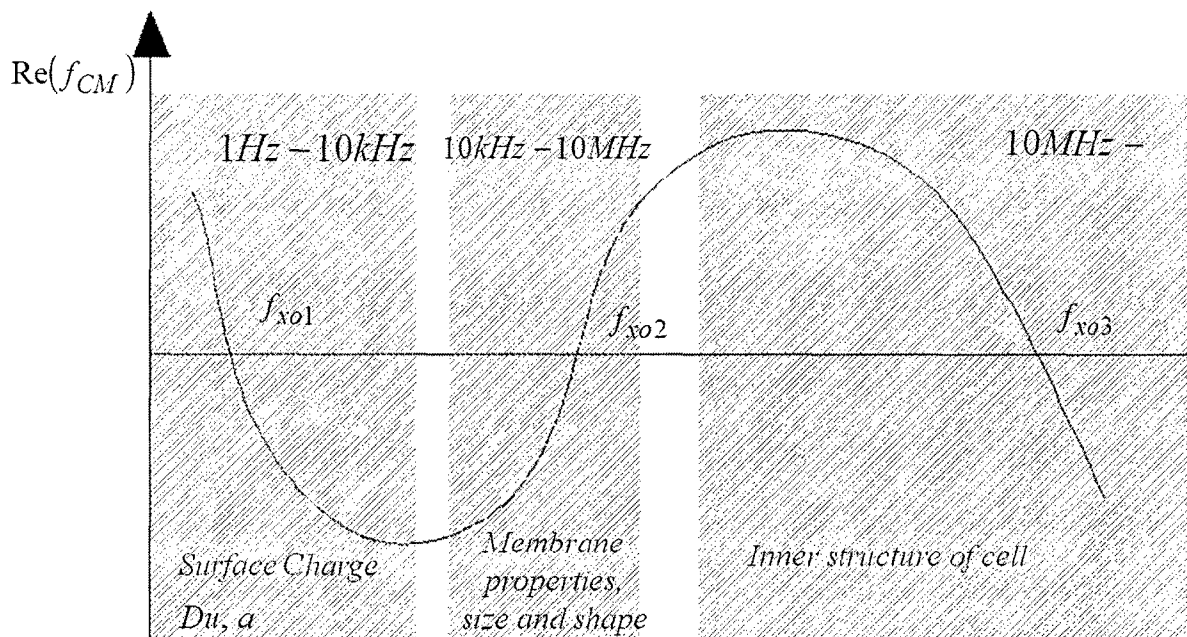 lower protein content and higher lipid content. The outermost structure of biological cells and cell organelles is the plasma membrane. The cell membrane is a key element in the life cycle of the cell; it regulates important functions of the cell. Even the simplest forms of life, such as bacteria, bear a cell membrane. More specifically, the cell membrane is a border at the periphery of a dynamic environment that produces metabolites, reproduces, and acquires fundamental organic and inorganic compounds from the environment. A typical cell membrane is schematically shown in figure 2.9. The main constituents of the cell membrane are the lipid bilayer and proteins. The bilayer is formed from two layers of lipid molecules with their hydrophobic hydrocarbon tails facing each other and hydrophilic heads facing inward or outward from the cell. The bilayer nature of the cells is energetically favorable state as the hydrophilic heads tend to touch water and hydrophobic tails aggregate. A cell membrane bears several other molecules such as carbohydrates and cholesterol. Interestingly, a cell membrane has also been observed to be in a fluid phase, allowing lateral transport of several elements around it. Functions of the proteins in (cytochrome-b), on (spectrin) or extending across (glycophorin, Na-ATPase) the cell membrane can extend from regulating the transport of species through the cell's membrane to linking intracellular actin filaments to extracellular matrix proteins. The cell membrane permits diffusion of small nonpolar molecules and uncharged polar molecules through it. Water, O_2, CO_2, ethanol, and glucose can pass through the cell membrane by diffusion; however, transport of all charged molecules and ions is regulated by proteins. The transport of

charged species can occur either through the ion channels or by transporter proteins that undergoes conformal changes to transport them. The mechanism of transport can be either passive, which means that it is driven by electrochemical potential, or active (happening against an electrochemical potential). Active transport needs energy input in the form of ATP (Adenosine Triphosphate, the main compound in a cell that transports chemical energy) hydrolysis or can be coupled to some other species' transport. Usually the cell maintains certain molecules in the cytoplasm and expels some to the outer environment. For example; K^+ ions may enter in the cytoplasm; however, a cell can be more selective against Na^+ ions. As a consequence; a cell maintains a membrane potential; that is, by generating different charge densities inside and outside the cell membrane. Membrane potential is a key factor in membrane transport of ions. While the cell interior is more negatively charged, outside the cell is cation rich. The membrane potential is negative and around -20 to -200 millivolts, depending on the cell type.

Although the structure of the plasma membrane is complex and bears various components, a lower order model to represent the membrane is a bimolecular lipid leaflet. The overall thickness of such a structure would be on the order of 5-10 nm, which is also confirmed by electron microscopy. The relative permittivity of the membrane can be estimated to be between 2 and 2.2 if the membrane is assumed to be composed of pure lipid matrix (Wang et al., 1994). Also for lipid-protein matrix the specific resistivity of the membrane will be on the order of 10^{12} ohm·cm (Pethig, 1979). In addition, ionic transport across the cell membrane and lateral transport around the cell has substantial effect on membrane conductance. Specific capacitance, total capacitance, and resistance of the cell membrane can be calculated by the following equations, respectively:

$$C_{spec} = \frac{\varepsilon \varepsilon_0}{t} \qquad (40a)$$

$$C_{tot} = 4\pi a^2 C_{spec} \qquad (40b)$$

$$R_{mem} = \frac{t}{\sigma_{mem}} \qquad (40c)$$

Using the permittivity value given above the estimate of the specific cell membrane capacitance will be on the order of 0.8 μF/cm^2 for an average cell, whereas capacitance values given in the literature are on the order of 1 μF/cm^2. The discrepancy between the estimation and the measurement can be attributed to the presence of the various components in the cell membrane. Cholesterol was shown to have little effect on membrane dielectric properties (Fettiplace et al., 1971). A relative permittivity of 2.8 can be assigned to hydrophobic non-polar aminoacids of integral, transmembrane proteins (Wang et al., 1994). The specific membrane capacitance can be calculated to be on the order of 1 μF/cm^2 if proteins composed 40% of the plasma membrane. The micro-structures on cell membrane, such as microvilli, blebs, folds, and ruffles, were also shown to affect the total cell membrane capacitance by increasing the surface area (Sukhorukov et al., 1993; Wang et al., 1994; Huang et al., 1996; Pethig et al., 2002). The presence of water in aqueous pores of the membrane has little effect on the membrane capacitance, and therefore can be neglected (Pethig and Kell, 1987). Prodan (Prodan and Prodan, 1999; Prodan et al., 2008) modeled α and β dispersion in biological cells, which yielded analytical solutions for the complex polarizability of cells. The model includes a single shell representing the cell membrane. Furthermore, they considered the singular current

as a result of the lateral transport of free charge. One of the important parameters in their

model is the membrane potential, which is given as,

$$\Delta V = \frac{k_B T}{q_s} \frac{\sigma_{sf}}{D} \frac{A_{mem}}{C_{mem}}, \tag{41}$$
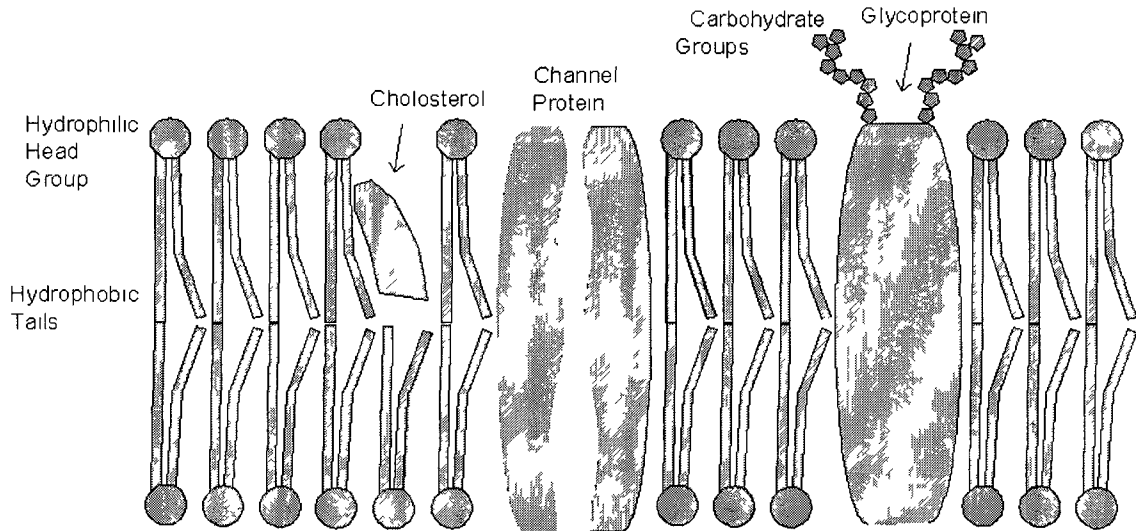
Figure 0.9 Schematic structure of a typical cell plasma membrane

where q_s is the surface charge density, σ_{sf} is the conductivity of the superficial charge

on the membrane, and A_{mem} and C_{mem} are the total area and capacitance of cell

membrane, respectively. The authors demonstrated that membrane potential and mobility

of the surface charge controls α dispersion, and conductivities of the medium and cytosol,

and membrane thickness controls β dispersion. Later Di Biasio and Cametti (Di Biasio

and Cametti, 2010b) extended this model to account for large surface charge densities

and for the conductivity of the membrane. In another work, the same authors investigated

the polarization of spheroid geometries (Di Biasio et al., 2010). However, without

consideration of double layer and the fields associated with it, the estimate of α

dispersion is incomplete. Stoneman et al. (2007) investigated the influence of proteins in

the plasma membrane on the cell polarizability in the frequency range up to 100 MHz by genetically modifying a yeast cell to over-express a specific protein in the plasma membrane. The results were surprising, as the number of the proteins in the plasma membrane was shown not to influence the cell polarizability in the low frequency region. However, it was suggested that non-linear dielectric spectroscopy (where ε_{mem} is now a function of $\bar{E}$) can capture changes in the membrane proteins after an applied electric field. In addition, nonlinearity of the cell membrane was shown to affect the electromechanics of the cells (Paddison et al., 1995). There are several studies that probed cell dielectric responses at low frequencies. The dielectric changes following a pulsed electric field (Zhuang et al., 2009); dielectric characterization of highly and poorly metastatic neck cancer cell lines (Cho et al., 2009); D-glucose induced changes in cell membrane permittivity (Di Biasio and Cametti, 2010a); dielectric spectroscopy of blocked and unblocked K^+ and Ca^{2+} ion channels in chromaffin cells (Han and Frazier, 2006) have all been studied in the Maxwell Wagner polarization range (up to 100 MHz).

2.4 Electromechanics

Electromechanics investigates forces and torques on particles (usually of sizes less than 1 mm) that are induced by electric or magnetic fields. Dielectrophoretic force that arises when a dielectric particle is put in a non-uniform electric field, and electrorotational torque that arises when a dielectric particle experiences a rotating electric field will be investigated in this section. Magnetophoresis and Quincke rotation are other types of effects that fall under electromechanics; however, these will not be addressed in this work. Both dielectrophoresis and electrorotation have important applications spanning

from particle characterization to manipulation. The corresponding literature reviews will be provided at the end of each sub-section.

2.4.1 Dielectrophoresis Theory

In this section, induced dipole moment of a uniform solid spherical particle in a uniform electric field is derived, and then using this dipole moment, the time averaged DEP force is obtained. Although DEP force occurs for a particle in non-uniform electric field, for ease of derivation a uniform electric field around a dielectric particle is assumed. The effective dipole method, which is followed in the derivation of DEP force, is valid only if the electric field non-uniformity is much larger than the characteristic length, which is the particle radius. We refer to utilization of the Maxwell stress tensor for the derivation of DEP for electric fields having an arbitrary order of non-uniformity (Wang et al., 1997). We assume that a dipole of $+Q$ and $-Q$ separated by distance d is placed in a non-uniform electric field as shown in figure 2.10. The net electrostatic force on it will be,

$$\bar{F} = Q\bar{E}(\bar{r} + \bar{d}) - Q\bar{E}(\bar{r}). \tag{42}$$

If d is small compared to non-uniformity in the system, the E field in the first term of the above equation can be expanded around an arbitrary point (r in the neighborhood of d) by the Taylor series. The net electrostatic force then becomes,

$$\bar{F} = Q\bar{E}(\bar{r}) + Q(\bar{d} \cdot \nabla)\bar{E} + h.o.t. - Q\bar{E}(\bar{r}). \tag{43}$$

In the above equation *h.o.t.* represents higher order terms, which can be neglected to some accuracy. If we put the dipole moment in and neglect the higher order terms, the equation becomes,

$$\overline{F}_{DEP}(t) = (\overline{p}(t).\nabla)\overline{E}(t), \tag{44}$$

where *p* is the polarization vector that was formulated previously for a spherical particle in equation 12. The time averaged force on the particle then becomes (Jones, 1995),

$$\left\langle \overline{F}_{DEP} \right\rangle = 2\pi\varepsilon_m a^3 \, \text{Re}(f_{cm})\nabla E_{RMS}^2, \tag{45}$$

where $\left\langle \; \right\rangle$ represents time average and E_{RMS} is the root mean square of the external electric field. This force is named as *dielectrophoresis* by Pohl in 1951 (Pohl, 1951). This approach is only an approximation of particle motion in a non-uniform electric field; a more rigorous approach includes particle multipoles that occur when electric field non-uniformity is high. A generalization of the dielectrophoretic force to include particle multipoles is given in the textbook by Jones (Jones, 1995). In addition, if polarization mechanisms other than the Maxwell-Wagner mechanism are present, the Clausius-Mossotti factor in equation 45 should be replaced by the general expression given by equation 14. Dielectrophoresis has been used extensively to separate, build, and characterize colloids and nanostructures. A recent review by Pethig (2010) summarizes the status of research on dielectrophoresis. Crossover frequency measurements have been used to probe biological cells undergoing chemically induced apoptosis (Pethig and Talary, 2007; Wang et al., 2002). The crossover frequency is the applied field frequency at which the particle exhibits zero net motion and it is given as (Jones, 1995),

$$f_{xo} = \frac{1}{2\pi} \sqrt{\frac{(\sigma_p - \sigma_m)(\sigma_p + 2\sigma_m)}{(\varepsilon_p - \varepsilon_m)(\varepsilon_p + 2\varepsilon_m)}} \cdot \qquad (46)$$
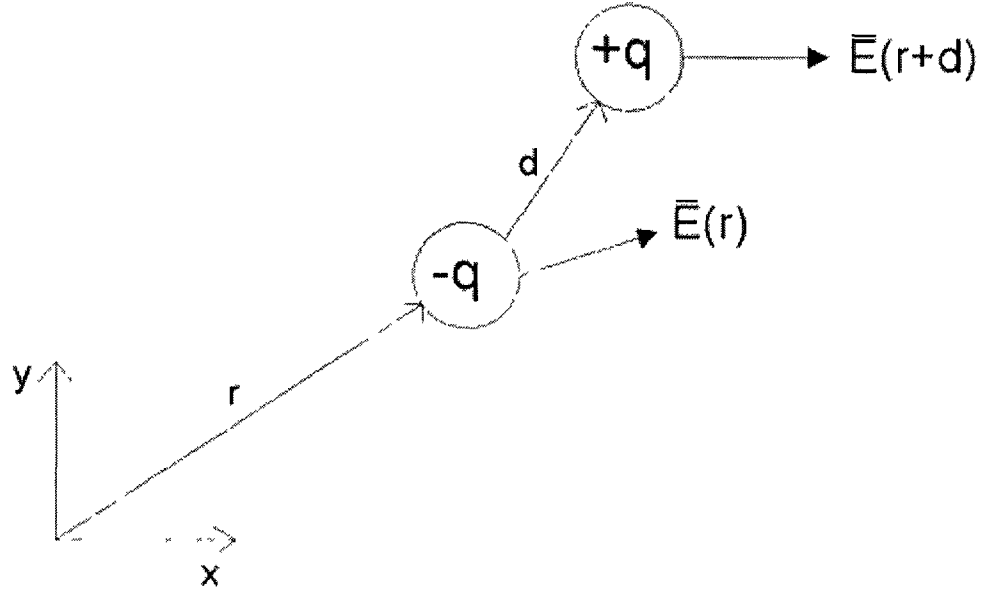
Figure 0.10 A dipole in a non-uniform electric field

For biological cells the above equation can be simplified as (Huang et al., 1996),

$$f_{xo} = \frac{\sqrt{2}\sigma_m}{2\pi r\, C_{mem}} \sqrt{1 - \frac{G_{mem} R}{2\sigma_m} - 2\left(\frac{G_{mem} R}{2\sigma_m}\right)^2}, \qquad (47)$$

under the following assumptions,

$$\varepsilon_m \ll \tilde{\varepsilon}_{cell},$$

$$\varepsilon_{cell} = R C_{mem},$$

$$\sigma_{cell} = R G_{mem},$$

where C and G are the capacitance and conductance, respectively. These assumptions are valid for field frequencies well below the interfacial relaxation frequency, which is at

several hundred kHz for typical mammalian cells in low conductive buffers (~10 mS/m). Cell properties (C_m and G_m) can be found by following an optimization algorithm, which minimizes,

$$\Delta = \sum_{i}^{N} (f_{xo,theory} - f_{xo,\exp})^2 ,$$

where N is the number of experimental data. Theoretical expression for the crossover frequency is obtained from equation (47) through estimation of C_m and G_m. For the determination of the experimental crossover frequency, first cell velocities at different frequencies are measured by video microscopy. The measured velocities are normalized by electric field gradient and particle radius. Assuming the cells are perfectly spherical and the focal plane is at the symmetry plane of the cell, the cell radius is readily measurable by video microscopy. The electrostatic limit can be assumed for electric field simulations, and hence, Laplace's equation can be solved for the electric potential in two dimensions. In simulations, electric potentials will be prescribed on electrode boundaries and side boundaries will be taken as symmetric. Then a curve can be fit to field frequency vs. normalized cell velocity data. The curve will be in the form of $\mathrm{Re}(f_{CM})$ that is,

$$\mathrm{Re}(f_{CM}) = A \frac{\left(1 + B\omega^2\right)}{\left(1 + C\omega^2\right)}, \tag{48}$$

where A, B, and C are arbitrary parameters. Crossover frequency will be the intercept of the curve at the field frequency axis.

2.4.2 Dielectrophoresis Applications

The direction of the dielectrophoretic force on a particle suspended in a fluid depends on the ratios of the complex permittivities of the particle and the fluid. As a result, particles of similar sizes but with different electrical properties can be separated and trapped by an alternating electric field depending on the frequency and electrode geometry (Pethig and et al., 1992). Applied to mammalian cells with dissimilar dielectric properties, this method permits separation of heterogeneous populations of cells (Becker and et al., 1994; Gascoyne et al., 1997; Talary et al., 1995). Therefore, if the dielectric properties of a specific cell type are known, the presence of these cells in a given sample, e.g. blood smear, can be determined. As a result, dielectrophoresis offers a fast diagnostic tool to screen for diseases that changes electrical characteristics of cells. Cancer cells especially have been found to differ significantly from their normal counterparts in their dielectric properties (Polevaya et al., 1999a). This opens the possibility to utilize a dielectrophoretic diagnostic tool to separate cancer cells, especially when they have already entered the blood stream or the lymphatic system (metastasis). In addition to the metallic electrodes that are being produced by chemical deposition techniques, indium tin oxide (ITO), which is applied as a thin film over a substrate, can be used as electrodes. The optical transparency of ITO electrodes is high, which enables particle observation on electrodes by transmission light microscopy. Several studies utilized ITO electrodes, for instance, to separate colorectal cancer cells using planar angled ITO electrodes (Yang et al., 2010). One other study utilized ITO as ground electrode in a continuous cell sorting device (Li et al., 2007). The electrode configuration for continuous sorting of target cells in a heterogeneous population can be either an angled design that exerts a lateral force on the

target species (Cheng et al., 2007), or a face to face design that produces vertical forces on particles of interest (Schnelle et al., 1999).

DEP trapping and sorting of particles are often limited by a lower field frequency limit around ~1 kHz. Measurements below ~1 kHz are affected by electrochemical reactions occurring on electrode surfaces. In order to overcome this problem, insulating materials are used instead of metal electrodes that can cause constrictions and dilatations in the electric field and hence field gradients (Chia-Fu and Zenhausern, 2003; Kang et al., 2009). This technology eliminates the need for metal evaporation; it is chemically inert and mechanically robust. A recent review by Pethig (Pethig, 2010) summarizes the status of research on dielectrophoresis. In addition to the particle sorting and trapping by dielectrophoresis, electrical properties of target cells can be estimated by measuring the crossover frequency. Crossover frequency measurements have been used to probe biological cells undergoing chemically induced apoptosis (Pethig and Talary, 2007; Pethig et al., 2002). According to Wang et al. (Wang et al., 2002), this method yields better results than surface phosphatidylserine expression or DNA fragmentation during apoptosis. One other study investigated the effect of melanin content of mouse melanoma cells on crossover frequency (Sabuncu et al., 2010).

2.4.3 Electrorotation

Electrorotation is the rotation of polarizable particles in linear (Quincke rotation) or rotating fields. The direction and rate of rotation is dependent on the particle polarizability and the constant phase lag between the electric field vector and the polarization vector. The torque on a particle in a time varying electric field is,

$$\bar{T}(t) = \bar{p}(t) \times \bar{E}(t). \tag{49}$$

If a particle is put in a rotating electric field that is (figure 2.11),

$$\bar{E} = E(\hat{x} - i\hat{y}), \tag{50}$$

The time averaged torque on the particle becomes (Jones, 1995),

$$\langle \bar{T}(t) \rangle = -4\pi\varepsilon_m a^3 \, \mathrm{Im}(f_{cm})E^2\hat{z}, \tag{51}$$

where *Im* represents the imaginary part. In steady state, this torque can be equated to the hydrodynamic drag force given by (Currie, 2002),

$$T_\mu = -8\pi \mu a^3 \Omega. \tag{52}$$

where Ω is the steady angular velocity of the particle. One important aspect of analysis using particle rotation is the existence of multiple solutions for the angular velocity. For particles suspended in low viscosity medium and when the polarization vector precedes the electric field vector there are multiple solutions to the angular velocity. This issue is investigated in the textbook by Jones (Jones, 1995).

Electrorotation has become a standard tool in dielectric spectroscopy of single cells. Usually particle rotation speed is recorded against changing medium conductivity and applied electric field frequency by keeping the electric field strength constant. The resulting curves are fitted by optimum values of cell properties. Sukhorukov et al. (1993) measured hypotonically induced membrane capacitance changes by electrorotation. Yang et al. (1999) measured dielectric properties of human leukocyte subpopulations by

electrorotation and correlated the membrane capacitances to the surface morphologies determined by SEM.
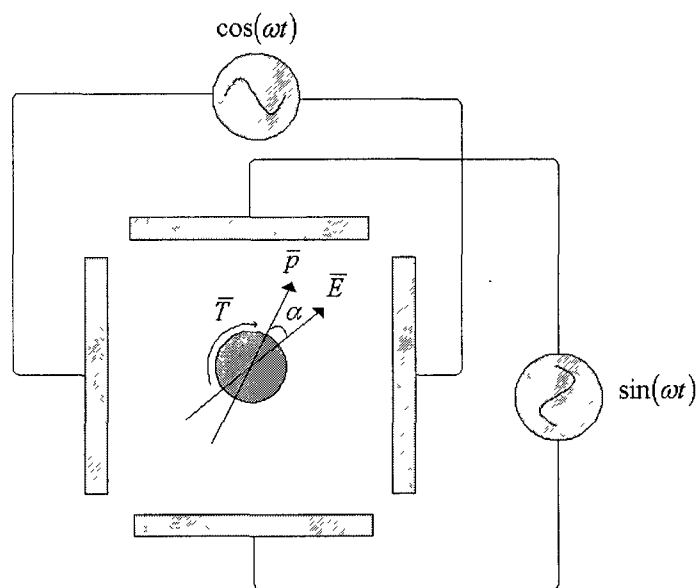
Figure 0.11 A particle in a rotating electric field

Although electrorotation and dielectrophoresis appear to be attractive methods to measure dielectric properties, they have their own disadvantages. The first drawback is the electrothermal fluid motion induced by the external applied field. Usually the electrothermal motion is significant for a high conductivity medium and at high applied voltages. Also, at high values of medium conductivity (~0.1 S/m) the medium is always more polarizable than cells, resulting in negative values of the Clausius-Mossotti factor regardless of field frequency. In this situation the crossover frequency cannot exist. Because of these facts, cells are usually suspended in a low conductivity medium (electromanipulation buffers) that might cause additional effects on cells such as osmotic swelling. In addition, the drag on particle rotation (equation 52) needs to be corrected to

account for the wall effects, or the particle has to be levitated to a suitable distance from the substrate (Reichle et al., 1999).

2.5 Overview

In this chapter, polarization of colloidal particles with particular attention to the double layer polarization and polarization of biological cells is addressed. In the low frequency range (1Hz – 100MHz) two main dispersions were studied, namely α and δ dispersions. The Du number was shown to be the key factor in α (low frequency dielectric) dispersion of colloids. Maxwell-Wagner-O'Konski (δ) dispersion is a consequence of mismatch of the particle and medium dielectric properties, which occurs at particle boundaries. It has been stressed that there is no mixture model available that can account for the hydrodynamic interactions between particles. For biological cells, a single shell model was considered to effectively represent cells in the low frequency limit. The introduction of the cell membrane results in an extra dispersion (β dispersion). Cell membrane was shown to play an important role in β dispersion. Some theoretical approaches to model biological cells were presented. However, it should be noted that there is no available comprehensive model for low frequency cell polarization that can account for both complex cell membrane structure and the double layer.

CHAPTER 3

MATERIALS AND METHODS

In this section the methods that are utilized for the dielectrophoretic and impedance measurements will be presented. The materials and fabrication techniques of the devices are also addressed in this section. The chapter begins with microfabrication of the microfluidic devices and instrumentation of the experiments. The cell lines and growth conditions are listed. The chapter ends with the explanation of the numerical procedure to model the experimental data.

3.1 Microfabrication Methods

The schematics and pictures of DEP and impedance chips are shown in figure 3.1. The electrode geometries for DEP and impedance devices are obtained by standard photolithography techniques. Castellated type electrode geometry with 50 μm characteristic length is chosen for DEP studies. For both of the devices pre-cleaned microscope slides (Gold Seal micro slide, Gold Seal) are used as substrates. First, glass slides are cleaned in 1 M KOH and acetone in an ultrasonic bath. The slides are then rinsed with DI water (Simplicity, Millipore) and desiccated on a hot plate at 120 °C for 10 minutes. Positive photoresist (S1805, MicroChem) is spin coated on glass slides at 4000 rpm for 30 seconds for 0.5 μm photoresist thickness. Soft baking is applied on a hot plate at 120°C for 1 minute. The photoresist layer is exposed to 405 nm ultraviolet light (UV light source, Exoteric Instruments) for 3 seconds with an exposure dose of 11.74 mJ/cm^2. After keeping the wafers at room temperature for 5 minutes, the substrates are

then developed in MF24A developer for 1 minute. After rinsing the slides with DI water and subsequent baking, the slides are placed in plasma cleaner for 30 seconds to etch excessive photoresist. 10 nm-thick Cr and 50 nm-thick Au layers are deposited on the substrate using a metal sputtering chamber (K675XD, Emitech). By applying a lift-off process in acetone, the electrodes of DEP and impedance chips are fabricated. Micro-molds are manufactured by a computer numeric control machine tool. The spacers of DEP and impedance chips are obtained by casting Sylgard 184 (PDMS) silicon elastomer in micro-machined molds. The spacer for DEP chip has a thickness of 500 μm, the thickness of spacer for impedance chip is 250 μm. The DEP chips are sealed by vacuum grease to ensure no leakage. The impedance chips are fabricated by aligning two electrodes on top of each other and bonding them to the PDMS spacer that is in between. In this way a kind of parallel plate capacitor was formed. The PDMS is functionalized by exposing it to RF plasma for 1 minute at 600 mtorr and 30 watts. Strong binding occurred between glass and PDMS after joining them with slight pressure under a stereoscope. The inlet and outlet to impedance chambers were drilled by a diamond drill bit before joining the two pieces of electrodes. Cell suspensions are fed into the devices by using a pipette.

DEP chip is energized by connecting the terminals to function generator (AFG3102, Tektronix). The function generator is programmed to supply 180° shifted signals to two terminals of the device. The frequency and amplitude of the signal is adjusted from the control panel of the function generator. The impedance device is connected to high and low terminals to the impedance analyzer (High precision impedance analyzer, 4194A Agilent) in a 3 terminal configuration. Three aluminum plates and two isolated cables

with alligator clips are used as the test fixture (figure 3.1 (c)). By designing the fixture this way, the stray capacitance that is formed between cables and sputtered electrode pairs, and inductance of them is minimized. The impedance analyzer detects the impedance of the device by the auto-balancing bridge method; details can be found in the impedance measurement handbook by Agilent (Honda, 2009). Basically while two terminals of the impedance analyzer are supplying constant voltage, the other two terminals measure the current across the device.

3.2 Cell Lines

Dielectric spectroscopy experiments were performed on human costal cartilage chondrocytes, mouse melanoma B16F10, mouse hepatoma Hepa, and T-cell leukemia Jurkat cell lines (ATCC, Manassas, USA). The B16 and Hepa cells are grown in Dulbecco's Modified Eagle's Media (DMEM; ATCC, USA), Jurkat cells are grown in Roswell Park Memorial Institute Medium (RPMI; ATCC, USA), and chondrocyte cells are grown in chondrocyte growth medium (Cell Applications Inc., CA, USA). Both types of growth medium are supplemented with glutamine, penicillin, streptomycin and 10% fetal bovine serum and cells are grown in a humidified atmosphere with 5% CO_2 at 37°C. All the cells are suspended in isotonic buffer consisting of 229 mM sucrose, 16 mM glucose, 1 μM $CaCl_2$, and 5 mM Na_2HPO_4 in double distilled water (pH 7.4) for the experiments, after a washing step with isotonic buffer. The electrical conductivity of the isotonic buffers are adjusted by adding an adequate amount of phosphate buffered saline (PBS).
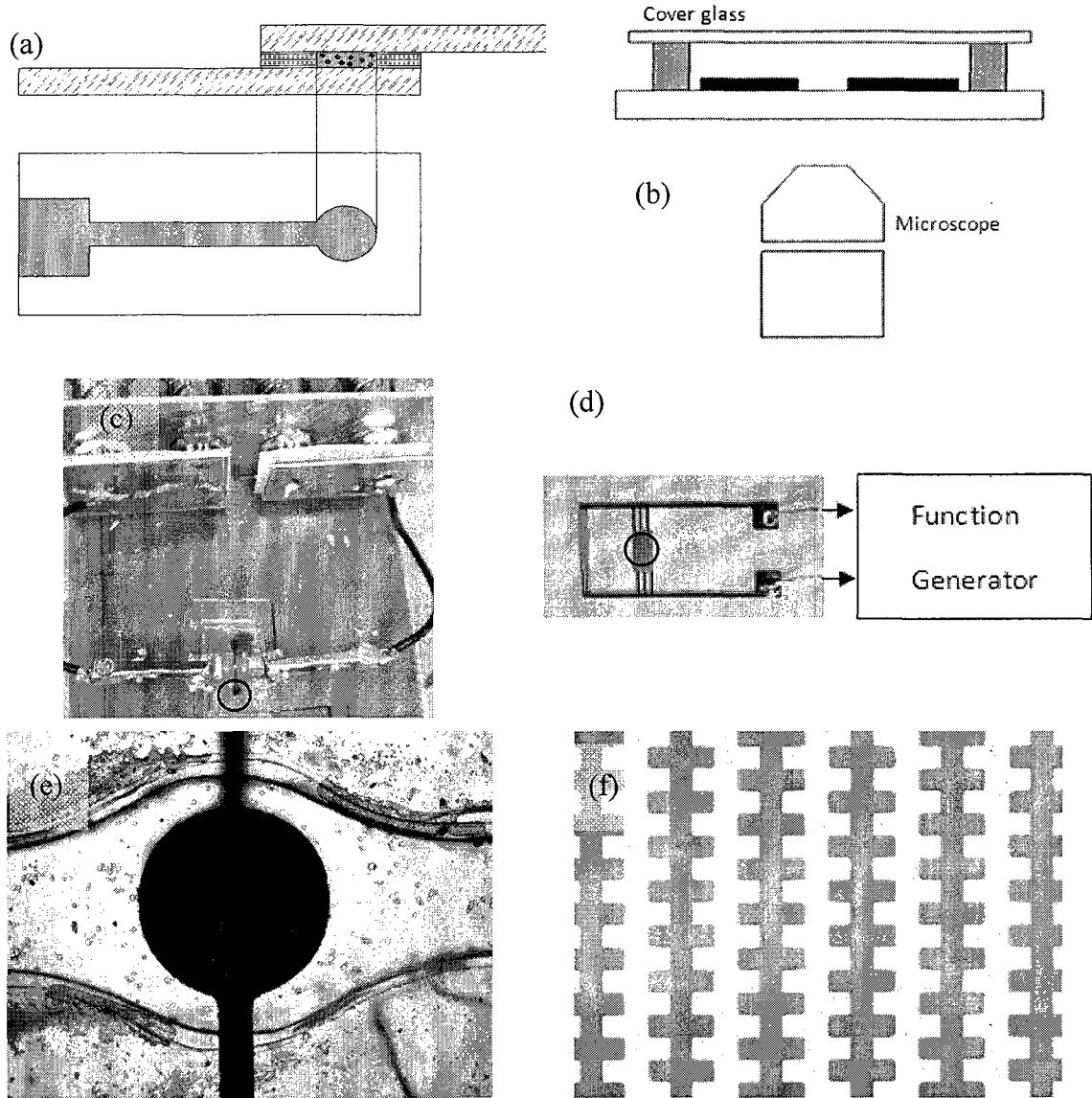
Figure 0.1 Pictures and schematics of microfluidic devices. Schematic view of impedance

chip (a). Top and bottom electrodes measure the impedance of the cell suspension in

between. Schematic view of the electrode array with a cover glass and PDMS spacer on it

(b). Microfluidic impedance chip filled with cells (c). Two non-touching gold arrays were

polarized by a function generator (d). Fluid and cell motion was observed by an inverted

microscope. Circular regions in (c) and (d) are viewed in detail. Closer views impedance

(e) and DEP (f) devices. Darker parts in (e) and (f) are electrodes.

Isotonic medium of 280 mOsm/kg was diluted by DI water to have hypotonic solutions for osmolarity experiments. Dilution by 60% and 80% with DI water yielded 224 and 168 mOsm/kg hypotonic solutions. The same cell suspension is used for all osmolarity experiments. Cells are centrifuged and re-suspended in hypotonic media. At each step cell concentration is determined by a hemocytometer.

In the modeling procedures all cells were assumed as perfect spherical particles. This is a reasonable approximation as cells become nearly spherical after non-spherical adherent cells were harvested from the culture flask by trypsinization. Cell size is determined by an image processing algorithm in MatLab (2011a, Mathworks). Cell radii are determined by calculating the area occupied by cells. The sensitivity of the cell radius measurements are 0.25 and 0.5 µm for Jurkat and chondrocytes cells, respectively.

3.3   Impedance Measurements

The impedance analyzer is calibrated at unknown terminals; it has a specific accuracy when the device under test (DUT) is connected to unknown terminals. However, the DUT does not always geometrically fit to the unknown terminals; several types of connectors and cables should be used between the DUT and the unknown terminals. The presence of the cables and connectors causes additional impedance sources other than DUT. They should be eliminated to yield the true value for the DUT. Open, short, and load compensation were performed to obtain the true impedance spectrum of the microfluidic device. As load, a standard 50 ohm resistor is used instead of a microfluidic device. For short and open measurements, alligator clips in figure 3.1 (c) are shorted and left open. All effects caused by the presence of extra equipment in the circuit can be

represented by an unknown 4-terminal circuit. Assuming that 4-terminal circuit is asymmetric, the true value of the DUT was calculated by the following formula (Honda, 2009):

$$Z_{dut} = \frac{(Z_{sh} - Z_{xm})(Z_{sm} - Z_0)}{(Z_{xm} - Z_0)(Z_{sh} - Z_{sm})} Z_{std},$$

(53)

where Z_{dut} , Z_{xm} , Z_0 , Z_{sh} , Z_{sm} , Z_{std} are corrected impedance of DUT, measured impedance of the DUT, measured impedance when the measurement terminals are open, measured impedance when the measurement terminals are short, measured impedance of the load device, and true value of the load device, respectively. Before analyzing any data obtained from the impedance analyzer, this procedure is performed to eliminate effects of the cables and the test fixture on the measured impedance. The corrected data consist of combined effects of lead resistance and inductance, stray capacitance, electrode polarization, and impedance of the suspension. The equivalent circuit that shows each element affecting the measured impedance is presented in figure 3.2. The first step towards fitting the data to existing models is to find the stray and unit capacitance of the device. Unit capacitance is a constant that is equal to $k A / d$, where k is a constant, A is the surface area of the electrodes and d is the separation between the electrodes. All complex permittivities that are determined by the fitting are derived utilizing unit capacitance, and therefore, exact dimensions of the device are unnecessary. Measurement of the chamber filled with deionized (DI) water and an empty measurement (air) are used to determine the stray and unit capacitance. Basically, as resistance of air is higher than that of DI water, the difference of reactance of DI water and air is proportional to the unit capacitance by a known constant. The values of the stray and unit capacitances are

checked by measuring the impedance of salt solutions with known conductivities. After finding the stray and unit capacitances the impedance spectrum is first fit into a model that consists of a serial combination of lead, suspension impedances, and electrode polarization effects. Electrode polarization is modeled by a constant phase element, and the formula is given by equation 23. For suspension the Cole-Cole model, which is described by equation 5, is used. The fitting procedure varied the values of the elements until the difference between the model and the measurement is minimized. From the first part of the fitting the parameters for electrode polarization (κ and α) and lead impedance (resistance R_L and L_L) are determined.
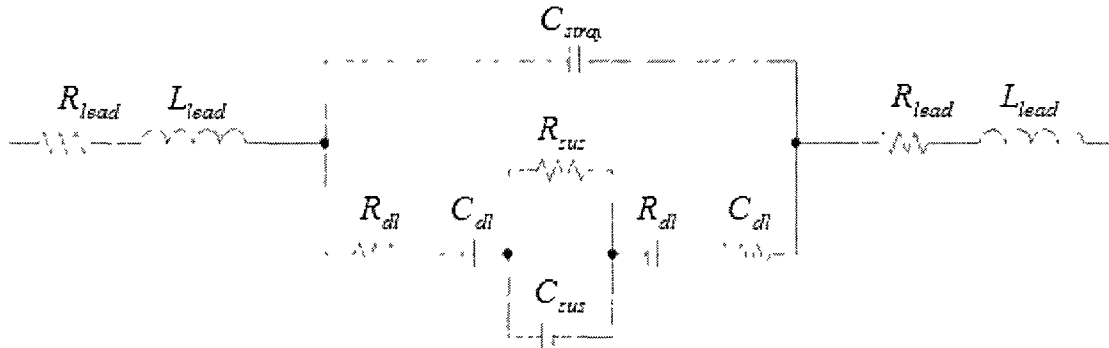
Figure 0.2 Equivalent circuit of the microfluidic device. Subscripts *dl* and *sus* stand for double layer and suspension, respectively

The capacitance values are verified with the measurements of the controlled salt solutions. The real and imaginary parts of measured and fitted spectra of 217 μS/cm (as determined by a conductivity meter) salt solution are given in figure 3.3 (a) and (b), respectively. The coefficient of variation of the permittivity and conductivity over 3 different measurements are given in figure 3.4. The coefficient of variation is defined as the standard deviation over the mean of the data ($c_v = \sigma_{std} / \mu_{mean}$). The coefficient of

variation is a measure of the variation of impedance data between measurements. According to figure 2.3, the relative change between the measurements is less than 0.1% for conductivity, and less than 2% for the permittivity. As the variations between experiments are less, it can be deduced that the precision of the device is good. The DC conductivity and relative permittivity of the salt solution was found as 79.69 and 216 μS/cm.

The measured permittivity is very close to that of water at $70°$ F (Kaatze, 1989). The second part of the fitting uses Maxwell-Wagner mixture (equation 11) and single shell (equation 11) models to fit the measured spectrum after accouning for the double layer and lead effects. The electrode polarization parameters obtained from the first fitting part are used in the second part. Certain parameters of cells in the single shell model are fixed in the fitting routine in order to increase the reliability of the fitting. The parameters that gave minimum difference between fitted and measurement data are used to characterize cells. The fitting procedures are performed in MATLAB® (2011a, Mathworks) using the nested *lsqonlin* function that utilizes an algorithm to minimize the sum of the squares of the residuals. The impedance data is averaged 4 times in the impedance analyzer before data acquisition. Also all the measurements except the cases for DEP and ion efflux quantification were taken at least 3 times using different suspensions.

DEP crossover measurements were also employed to extract dielectric properties of cells, and used to verify the cell parameters obtained from fitting. To a good approximation the second term in square root in equation (6) can be neglected; hence the crossover frequency becomes (Pethig et al., 2005),

$$f_{xo} \cdot r = \frac{\sqrt{2}}{2\pi C_{mem}} \sigma_{med} - \frac{\sqrt{2}G_{mem}r}{8\pi C_{mem}}.$$

(54)
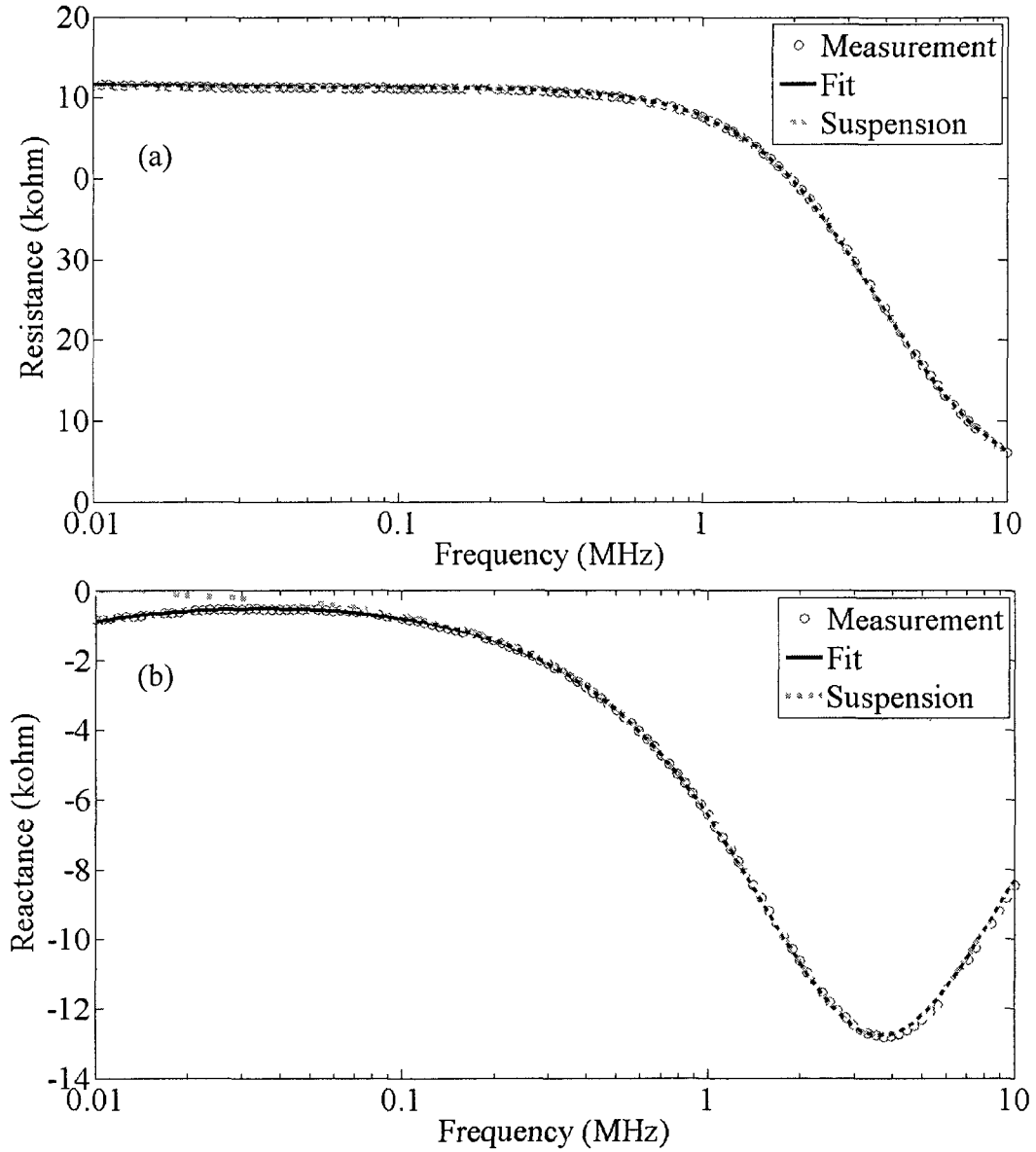
Figure 0.3 The measured and modeled resistance (a) and reactance (b) data for 217 μS/cm

salt solution. The dotted line represents the impedance spectrum of the suspension after

electrode polarization effects are removed

Figure 0.4 Coefficient of variation of 217 μS/cm salt solution dielectric measurement

In this section fabrication of the impedance and DEP devices is described. The methods used to derive cell properties from the raw impedance data are also described. In the next chapter, cell dielectric responses will be quantified using these methods.

CHAPTER 4

RESULTS AND DISCUSSION

In this section, dielectric properties of B16, Jurkat, and chondrocyte cells as extracted from dielectric spectroscopy and crossover frequency measurements are given. The dielectric parameters of Jurkat and chondrocyte cells are also measured and presented as a function of medium osmolarity. The ionic efflux from a cell line is quantified using the microfluidic device.
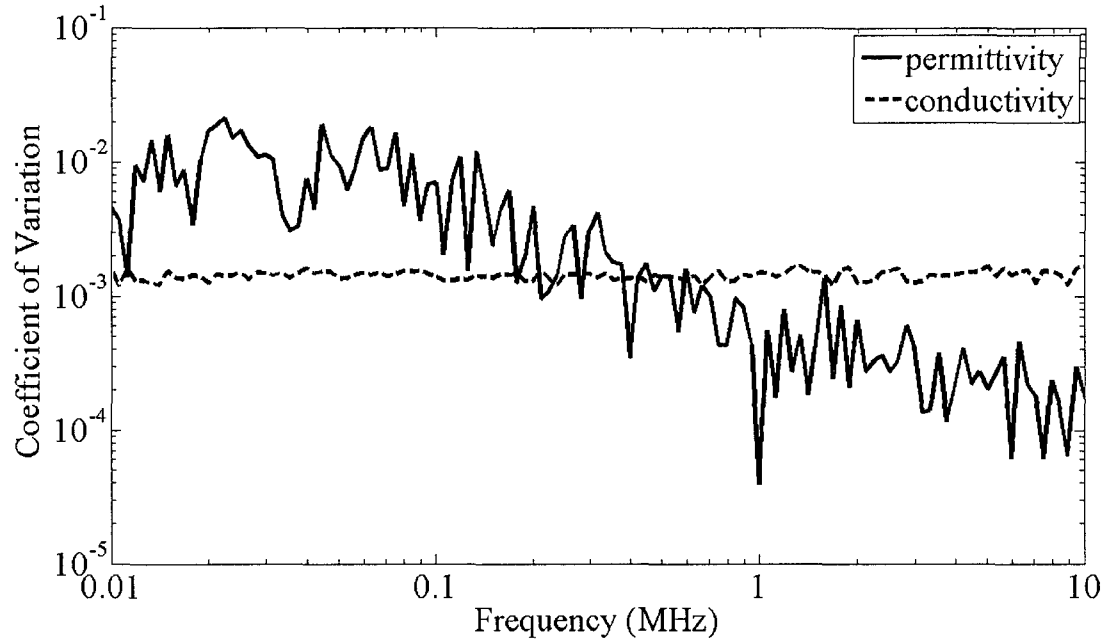
4.1 Measurement of Cell Dielectric Parameters

In table 4.1 the dielectric properties of Jurkat, B16, and chondrocyte cells are given. The coefficient of variations of Jurkat, B16, and chondrocyte cell suspensions' permittivity and conductivity between different repetitions are plotted in figure 4.1 (a), (b), and (c), respectively. According to the figure, the maximum relative error of the measurements is 2%. These suggest the high precision of the device. The impedance data acquired from the impedance analyzer is fitted to physical models to derive the properties of the membrane. The first part of the fitting procedure includes Cole-Cole and constant phase element models to describe the cell suspensions and double layer, respectively. While fitting the cell suspension, limiting low and high frequency values for permittivity (ε_s and ε_∞), relaxation time (τ_{rel}), and DC conductivity (σ) in the Cole-Cole model and κ and α in the constant phase element were set as variables. The second part of the fitting uses κ and α obtained in the first part of the fitting. A cell suspension is approximated as into one cell using the Maxwell-Wagner mixture model. Quantities for the cell membrane are
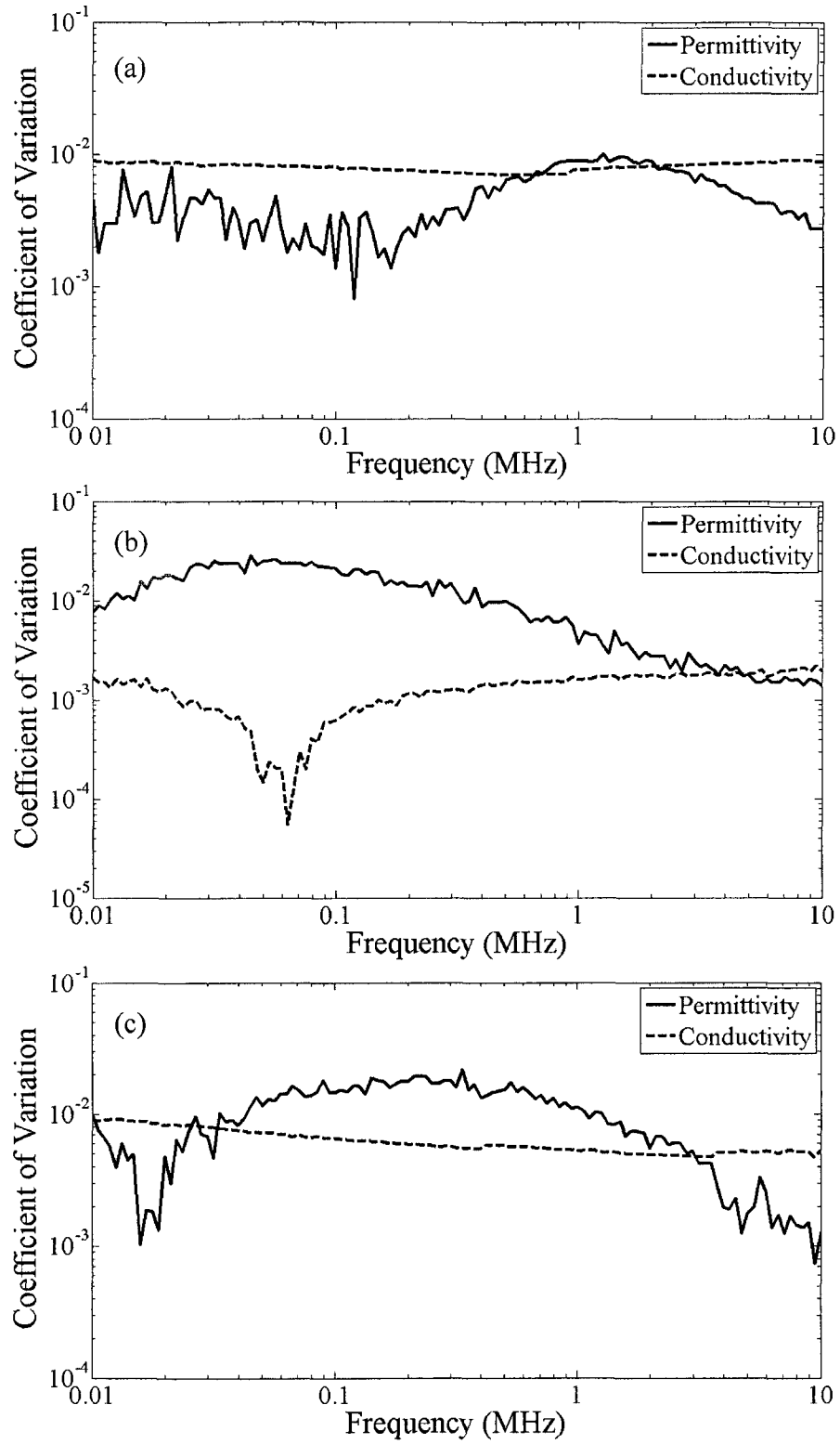
Figure 0.1 Coefficient of variation of Jurkat (a), B16 (b), and chondrocyte (c) cell

suspensions measurements

obtained by decomposing a single cell by the single shell model. The fitting algorithm used in this study to extract dielectric properties finds the local minima of the fitting function. This in turn allows several sets of variables to satisfy the convergence criteria. One way to reduce possible solution sets is to decrease the number of fitting variables; therefore, in this study only membrane properties are set to change in the fitting, as primarily membrane is probed in the frequency range (10 kHz – 10 MHz). Before fitting the raw data to physical models, these parameters are fixed to the constant values: $a, t, \varepsilon_{cyt}, \sigma_{cyt}, p$. The volume fraction of cells is denoted by p. Cell membrane relative permittivity (ε_{mem}) and conductivity (σ_{mem}) are set to change in the fitting process. The cell membrane permittivity and conductivity obtained from the fitting procedure and constants used for cells are summarized in table 4.1. Constants are marked by a star in table 4.1. According to table 4.1, chondrocyte cells have the largest membrane capacitance and membrane conductance. The membrane conductance of chondrocyte cells is more than 10 folds higher than those of Jurkat and B16 cells, while membrane capacitance is more than 2 folds higher than those of the other two cell types. The permittivity and conductivity spectra built with the values obtained from the fitting procedure and measurement data of the Jurkat cell suspension are plotted in figure 4.2 (a) and (b), respectively. In figure 4.2 (a) and (b) also the suspension permittivity and conductivity are plotted after extracting the effects of the double layer on electrodes. The root mean squares of the percentile errors in fitting of permittivity and conductivity are around 7% and 0.7%, respectively. In figures 4.3 and 4.4, suspension impedance spectra of B16 and chondrocyte cells are plotted, respectively. In (a) and (b) of figures 4.3 and 4.4 permittivity and conductivity of cell suspensions are presented, respectively. Raw,

modeled, and double layer effects corrected suspension spectra are shown in these figures.

Table 4.1 Dielectric properties of Jurkat, B16F10, and Chondrocyte cells

	Jurkat	B16F10	Chondrocyte
a [μm] *	6.1	7.5	9.2
C_{mem} [μF/cm^2]	0.69	1.67	3.74
G_{mem} [S/m^2]x10^3	3.78	3.5	39.85
C_{mem} [μF/cm^2]**	1.14	1.63	--
G_{mem} [mS/m^2] x10^3**	0.681	4.74	--
t [nm] *	7	7	7
ε_{cyt}*	60	60	60
σ_{cyt} [S/m] *	0.5	0.5	0.5
p [%]*	11	2.6	8

*these values are fixed during fitting

**values obtained by crossover frequency measurements

Cell membrane capacitance and conductance values are also measured by the dielectrophoresis crossover frequency measurement method. In figure 4.5, measured crossover frequencies at different medium conductivities are plotted for B16 and Jurkat cells, and also linear fits to the experimental points are shown. The cell membrane capacitance and conductance values that are obtained using this method are shown in table 4.1. These values are marked with a double star. According to table 4.1, the Jurkat cell membrane capacitance obtained from crossover measurements is higher than that derived from dielectric spectroscopy, while B16 cell membrane capacitance is lower than that derived from spectroscopy. However, both membrane capacitance measurement

Figure 0.2 (a) The measured and modeled permittivity (a) and conductivity (b) data for

Jurkat cell suspension. The dotted line represents the impedance spectrum of suspension

after electrode polarization effects are removed

Figure 0.3 (a) The measured and modeled permittivity (a) and conductivity (b) data for

B16 cell suspension. The dotted line represents the impedance spectrum of suspension
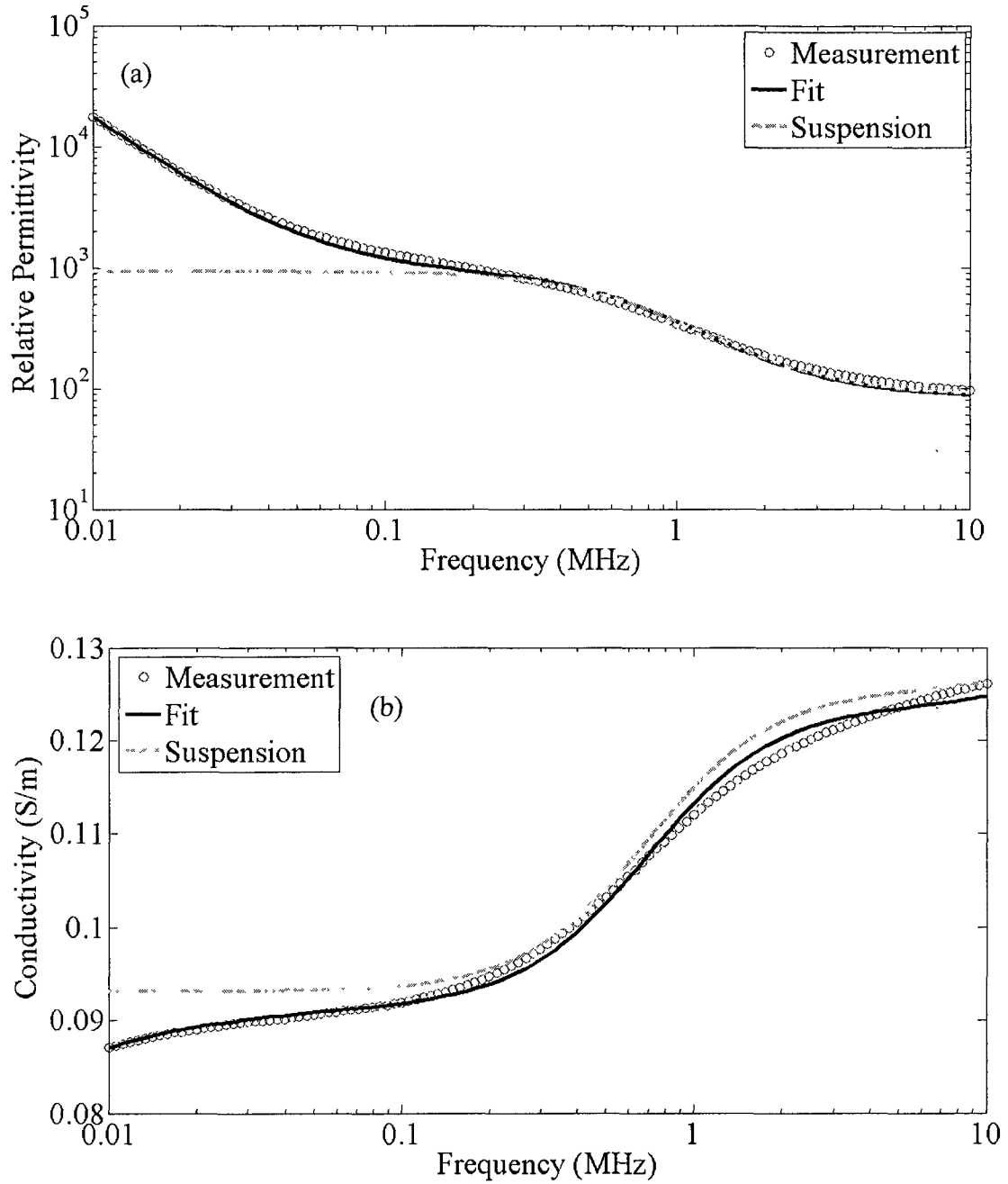
after electrode polarization effects are removed

Figure 0.4 The measured and modeled permittivity (a) and conductivity (b) data for

chondrocyte cell suspension. The dotted line represents the impedance spectrum of

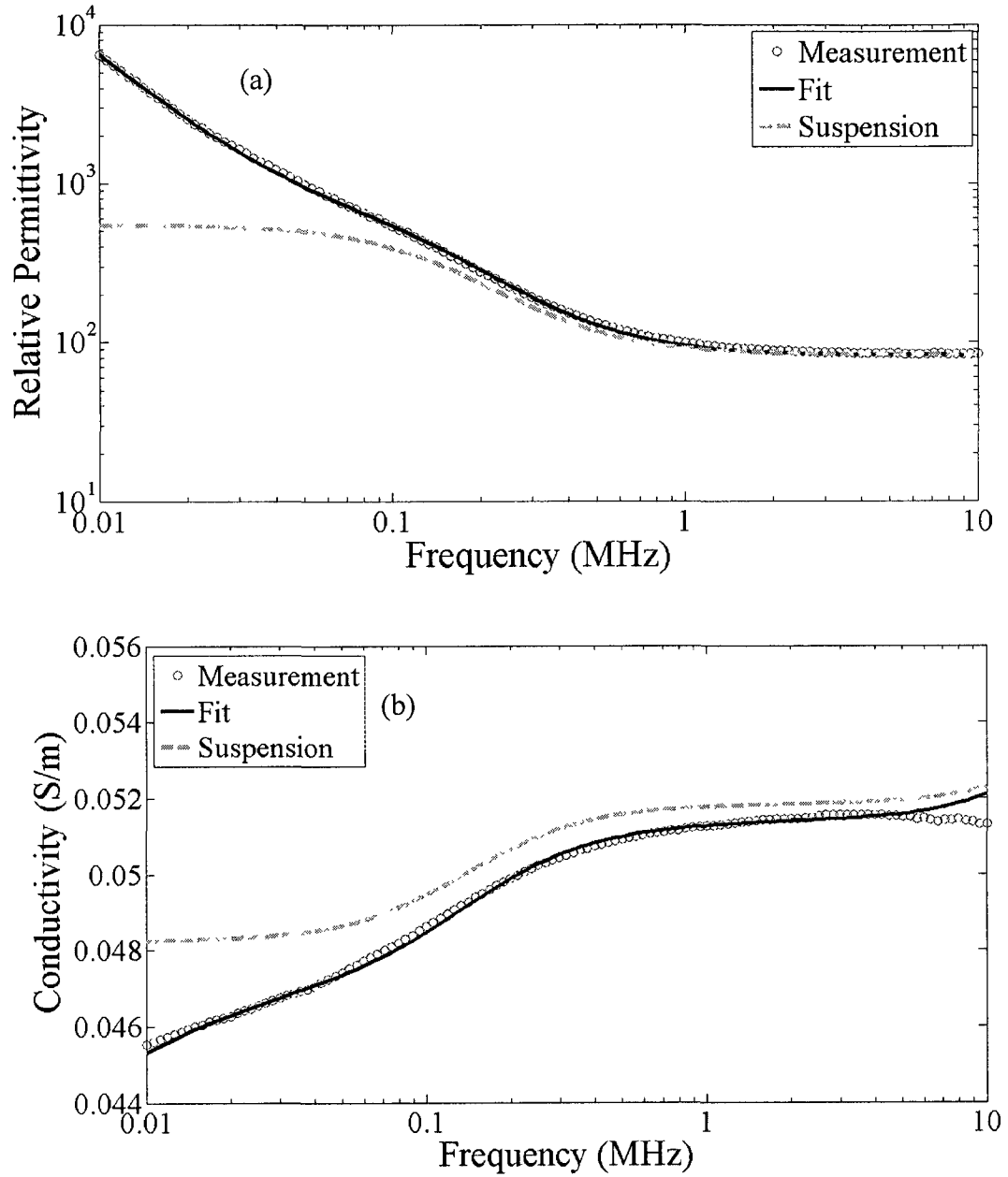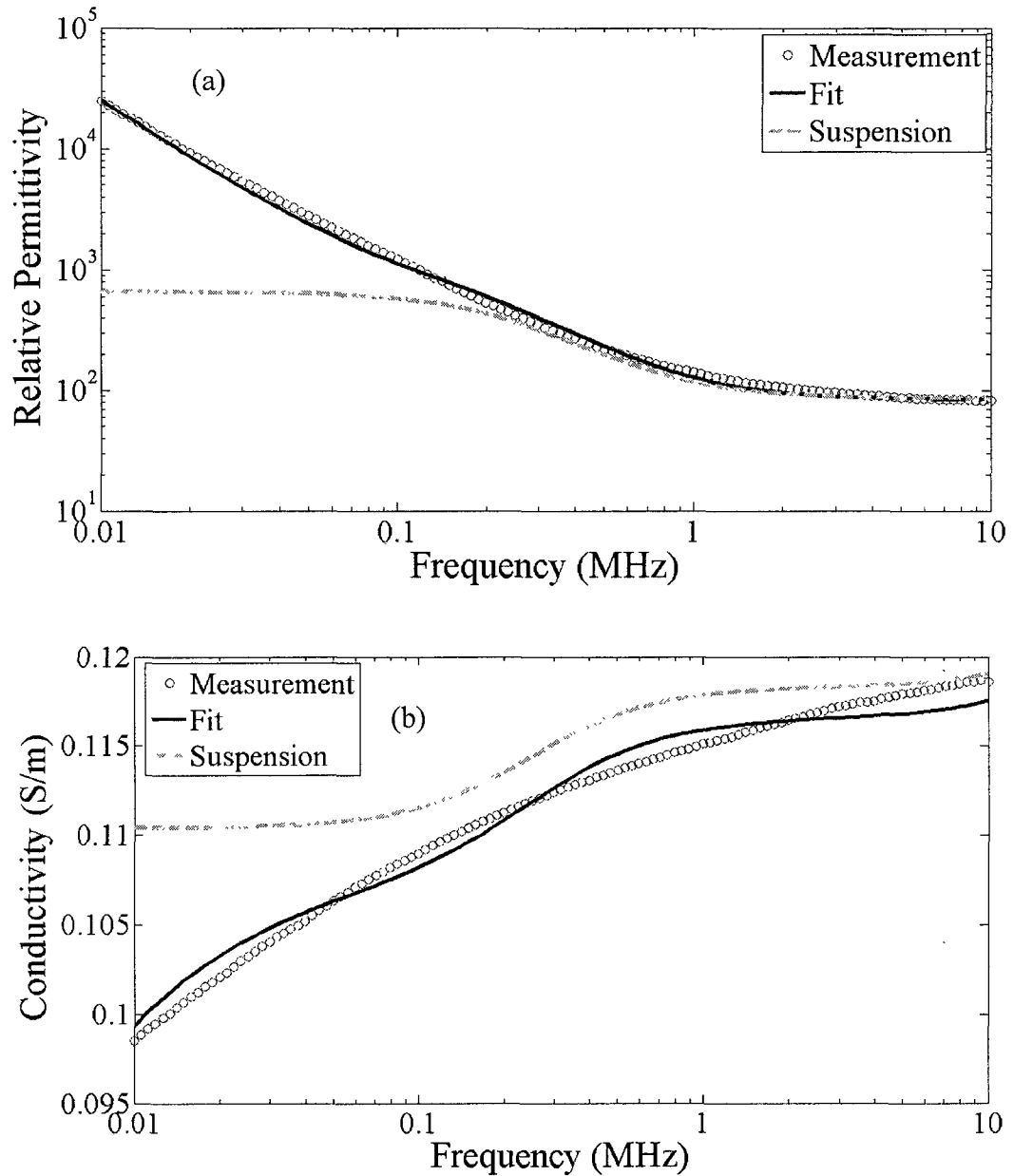suspension after electrode polarization effects are removed
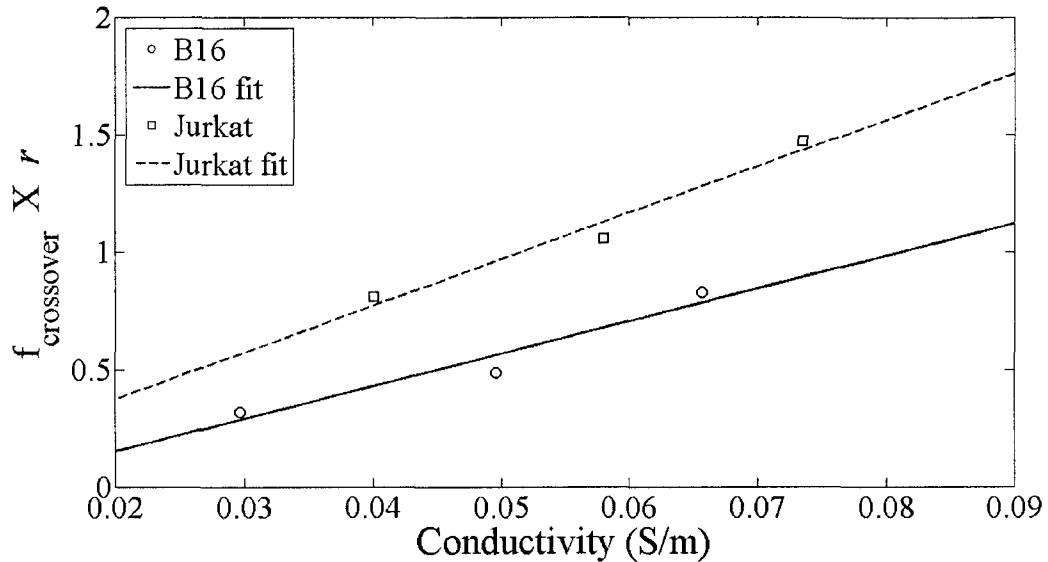
Figure 0.5 Crossover frequency measurements of B16 and Jurkat cells

methods follow the same trend, indicating that B16 cells have higher membrane capacitance. Membrane conductance of Jurkat cells obtained from the dielectrophoresis experiments are much lower than that derived from dielectric spectroscopy, while the value for B16 cells is in the same range as the value derived from spectroscopy.

Jurkat cells, a transformed T-cell leukemia line, are non-adhesive cells of small size with relatively little cytoplasm. The primary function of T-cells in the body is to recognize foreign objects and illicit an immune response. Conversely, B16 cells are derived from malignant melanocytes, and like many adherent cells, have a large cytoplasm and internal cytoskeleton to maintain cell properties. The dielectric properties of Jurkat cells found are in accordance with previously published reports on malignant T-cells (Ermolina et al., 2001, Garner et al., 2007). Chondrocytes are responsible for forming the extracellular matrix (ECM) of cartilage. Re-establishment of ECM as rapidly as 1-2 days was observed for chondrocytes that are plated on culture dishes (Kuettner et al., 1982). In tissue, chondrocytes are without cell to cell contact. Chondrocytes are surrounded by

highly negatively charged proteoglycans which attract large numbers of cations generating a high extracellular osmolarity. Chondrocyte cells are constantly exposed to gradients of pressure, ionic species, and electrical potential, and also they do not have a blood supply, which decreases extracellular pH. Chondrocytes respond to their unusual environment using their membrane transporters. For instance, articular chondrocytes regulate their volume to changing osmolarity by activating Na^+ - K^+ - $2Cl^-$ cotransporters and osmolyte channels on their membranes (Hall et al., 1996). The higher cell membrane conductivity of chondrocytes can be linked to their high number of membrane transporters.

The total membrane conductance per unit area can be decomposed into two elements (Pethig and Talary, 2007):

$$G_{mem} = \frac{2K_{sur}}{r^2} + G_{pores} .$$

(55)

K_{sur} is the membrane conductance that is associated with the electrical double layer of the cell. G_{pores} is the membrane conductance that is associated with ionic transport through pores. K_{sur} can be connected to Du number and zeta potential by equations 30 – 33. High membrane conductance of chondrocytes might also be linked to double layer conductance, which is function of cell surface charge magnitude. High membrane capacitance of chondrocyte cells can be associated with the high number of structural elements on the cell membrane, such as microvillus, blebs, ruffles, and folds (Yang et al., 1999). The morphologically rich cell surface contributes to higher membrane capacitance in the following way: The micro elements on cell surface increase total

surface area of cell. As the effective surface area of a cell increases, its charge holding capability increases. Higher charge storing capability results in higher membrane capacitance.

Dielectrophoresis experiments are also mainly carried out to verify the fitting results. However, even though fitting variables satisfy the crossover frequencies, this does not necessarily mean that they are the correct parameters. This problem is mainly due to the physical model used, as the single shell model cannot completely explain complex cell structure. Relative permittivity and conductivity values prescribed for the cytoplasm are approximations, and may change from cell to cell. Consequently, the values for the membrane are not exact, but rather approximate. Additionally, the single shell model assumes spherical cells, which in turn causes errors as cells are not perfectly spherical. A superior model would be double shell model; however, the double shell model introduces additional parameters to the fitting procedure, which in turn increases the number of possible solution sets.

The discrepancy between membrane conductance values obtained by crossover and dielectric spectroscopy measurements is mainly due to the former method's inability to determine membrane conductance. In other words, the crossover frequency measurement method is insensitive for the determination of membrane conductance. Equation 54 is used for extracting membrane properties from crossover measurements. The third term in equation 54, which holds the value for membrane conductance, is on the order of 10^{-2} while the other terms in equation 54 are on the order of 1. The value of the third term is also within the experimental error, if the error in determining crossover frequency is on the order of 1 kHz. Also crossover frequency variations between single cells in a cell line

can be larger than 1 kHz. This in turn prevents accurate determination of the membrane conductance from the crossover measurements.

4.2   Detection of Osmolarity Induced Changes

Dielectric spectroscopy was also used to probe changes in cell membrane to variations in osmolarity. Jurkat and chondrocyte cell suspension permittivity at 280, 224, and 168 mOsm/kg solutions is shown in figure 4.6 (a) and (b), respectively. For both cell suspensions the permittivities differ in the low frequency range. Close examination of Jurkat cell data (figure 4.6(a)) in the 0.1 – 1 MHz range indicates that the three cell suspensions have different time constants for β dispersion. The solid line in figure 3.4a that represents Jurkat cells suspended in isotonic buffer has larger dispersion. The data scales with the changing osmolarity; cells suspended in 168 mOsm/kg buffer have a sharper decrease from high to low permittivity. Cell size was also measured with changing osmolarity. Jurkat cell radii were measured as 6.1, 6.5, and 6.5 µm in 280, 224, and 168 mOsm/kg solutions, respectively. The cell viability was determined 96% and 94% for chondrocyte and Jurkat cells suspended in 168 mOsm/kg, respectively. The increase in cell size is due to increased cellular water uptake as the relative percentile of water in solutions increases. The cell membrane unfolded and flattened with increasing osmolarity; consequently, the membrane capacitance decreased. After a certain expansion, the membrane reaches its maximum flatness. On the other hand, the increase in the low frequency region of the permittivity spectra is mainly due to the cell size increase with osmolarity decrease. Cells become larger in hypotonic media; occupy more space, and increase cell suspension permittivity. The single shell model is fit to

experimental data to extract cell membrane conductance and capacitance. The membrane properties of Jurkat cells with changing osmolarity are given in table 4.2. According to the table, cell membrane capacitance and conductance decrease with increasing osmolarity. Cell membrane capacitance decrease is consistent with the observation made on cell radius. As cell membrane unfolds and the cell becomes larger, the charge storing capacity of the membrane and membrane capacitance decreases. The results on Jurkat cells are consistent with the previous studies carried out with different cell lines (Sukhorukov et al., 1993; Wang et al., 1994; Huang et al., 1995).

Table 4.2 Membrane properties of Jurkat and chondrocyte cells in different osmolarity solutions (Jurkat/chondrcocyte)

	280 mOsm/kg	224 mOsm/kg	168 mOsm/kg
C_{mem} [$\mu F/cm^2$]	0.69/3.81	0.65/3.66	0.64/3.51
G_{mem} [S/m^2]x10^3	3.78/40.55	1.94/32.64	0.19/28.68
a [μm]	6.1/9.2	6.5/9.2	6.5/9.2

Chondrocyte cells' response to changing osmolarity is shown in figure 4.6 (b). In contrast to the Jurkat cells' response, the data does not scale as 280<224<168 mOsm/kg in the low frequency range. Conversely, isotonic medium has the largest low frequency permittivity and the low frequency response scales with decreasing osmolarity. Chondrocyte cells did not show observable changes in size with changing osmolarity. The radius of the chondrocyte cells was determined as 9.2 μm. The differential response is most likely due to the differences in volume fractions between the suspensions. As cells are re-suspended, chondrocyte cells' response to changing osmolarity is shown in

figure 4.6 (b). In contrast to Jurkat cells' response, the data does not scale as

280<224<168 mOsm/kg in the low frequency range. Conversely, isotonic medium has
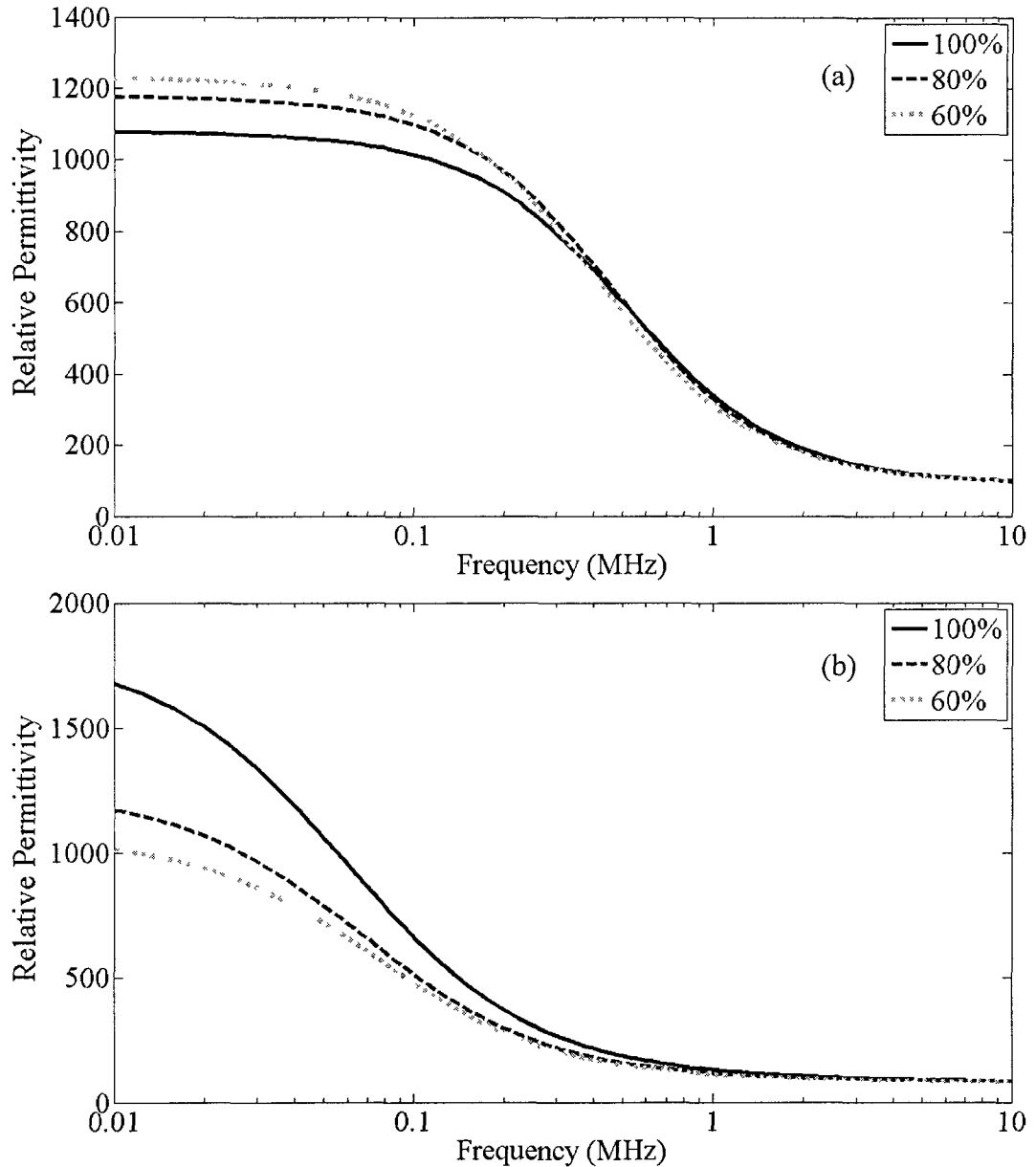

Figure 0.6 Suspension relative permittivity of Jurkat (a) and Chondrocyte (b) cells with

changing osmolarity. Isotonic 280 mOsm/kg solution is diluted by 80 and 60 percent to

obtain 224, and 168 mOsm/kg hypotonic solutions. Solid, dashed, and dotted lines

represent isotonic, 224 mOsm/kg, and 168 Osm/kg buffers, respectively

the largest low frequency permittivity and the low frequency response scales with decreasing osmolarity. As cells are re-suspended in new buffers some cells are lost during removal of the supernatant.

The cell membrane capacitance and conductance values for chondrocyte cells with varying osmolarity are given in table 4.2. Cell membrane capacitance and conductance slightly decreased with changing osmolarity, which is also the case for the Jurkat cells. Drop in the membrane conductance in Jurkat cells might be attributed to decreasing surface conductance. As cells swell in hypotonic media surface charge density decreases, and in turn, this causes decrease in the surface conductivity. However, as chondrocyte cells do not swell, further experiments such as zeta potential measurements are necessary to probe the surface conductance.

Bovine articular chondrocyte cell volume was previously probed with changing static and dynamic osmolarity (Grace Chao et al., 2005). According to the study, chondrocyte cells respond to the external stimuli in as little as 2 minutes. In addition, the isotonic medium osmolarity used in that study was 360 mOsm/kg, which is higher than the osmolarity of the isotonic buffer used in this study (280 mOsm/kg). Isotonic conditions of costal chondrocyte cells might be of a higher osmolarity value than that of Jurkat cells. Chondrocyte cells also possess a regulatory volume decrease mechanism to reduce the cell size following a hypotonic treatment (Hall et al., 1996). Following the facts listed above, at isotonic conditions used in this study (280 mOsm/kg), chondrocyte cells might have already expanded to their full extent or recovered to its original size. Further

experiments with confocal microscopy might also be necessary to observe minute changes in chondrocyte cell size.

4.3   Quantification of Ion Efflux

Cells suspended in low conductive buffers leak ions to external medium due to the electrochemical gradient across the cell interior and medium. The amount of ion leakage can be quantified in real time by impedance measurements. As the cells leak ions, the electrical conductivity of the external medium increases. The following equation can be written for the ionic concentration of the extracellular medium:

$$c_{med} = J \, n_{cell} t + c_o, \tag{56}$$

where c is the concentration, t represents time, J is ionic flux across the cell membrane, and n_{cell} is the cell concentration. J is assumed to be a function of time and uniform around the cell surface. Subscripts *med* and *o* stands for medium and initial state, respectively. Rearranging the above equation and taking the derivative with respect to time yields the following equation:

$$\frac{d\delta\sigma}{dt} = \Lambda n_{cell} A \frac{dJ}{dt} t + \Lambda n_{cell} A J, \tag{57}$$

where Λ is the molar conductivity.

Hepa cells are used to quantify the ion leakage due to availability. Cells are suspended in low conductivity buffer (0.0688 S/m) and the impedance of the cell suspension is measured for 1 hour at 5 minute intervals. Maxwell-Wagner mixture and single shell

models are used in combination as described before to derive extracellular conductivity. In figure 4.7 the conductivity increase of the extracellular medium of Hepa cells is plotted. A quadratic polynomial is fit to the experimental data. The coefficient of the leading order term (t^2) in the fitting polynomial is 4 orders of magnitudes less than the coefficient of the second order term (t). Therefore, the time dependent nature of ion flux can be neglected to a good accuracy. The time average flux from an average cell is estimated as 9.6248×10^{-12} [moles/s]. In the calculations only potassium and phosphate ions are assumed to transfer across the cell membrane (Gascoyne et al., 1993). This assumption follows the fact that the anions and cations that have the highest intracellular concentration are potassium and phosphate ions, respectively.
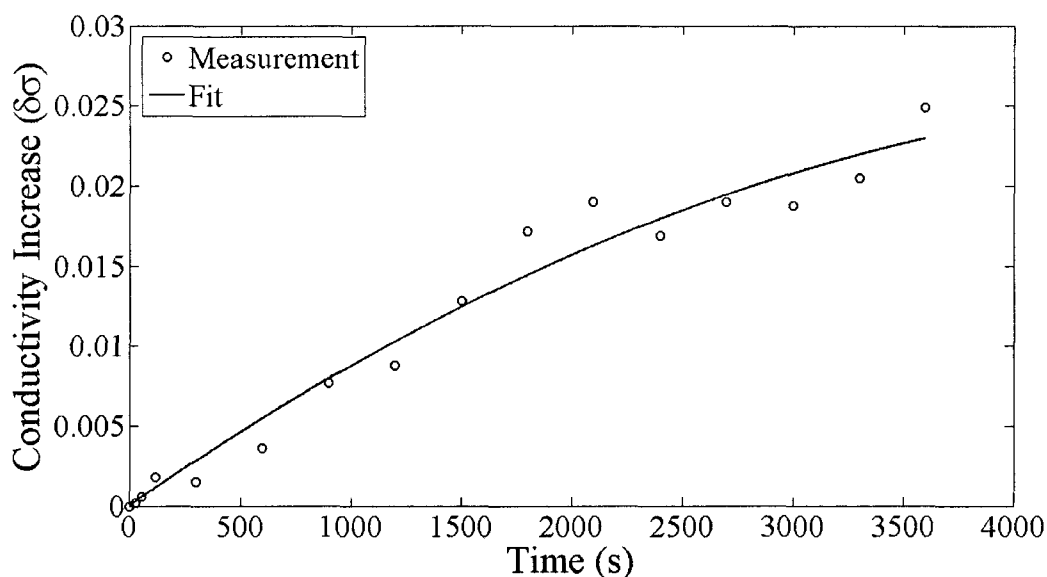

Figure 0.7 Conductivity increment in extracellular space of Hepa cells

4.4 Separability Parameter

Dielectrophoresis of cells can also be utilized to separate cells of interest from a mixed population. In order to have one cell type to be separated from the other, the polarity of

cells' CM factors should differ at fixed buffer conductivity and field frequency. In practice, selection of the field frequency is usually done by trial and error at a prescribed medium conductivity. Consequently, this process is time consuming, and selection of the medium conductivity is random. Selection of the highest possible conductivity that allows successful separation of cells is important for practical purposes. In order to overcome arbitrary selection of field variables and medium conductivity, a separability factor is introduced. The optimum separability is reached when there is enough difference between the particles' intrinsic properties.

For DEP force the effective parameters for cell separation are radius and Clausius-Mossotti factor, which are functions of the medium conductivity and field frequency. The separability parameter is defined as:

$$S_{12}(\omega) = \left| \left(a_1^3 \, \mathrm{Re}(f_{CM1}) - a_2^3 \, \mathrm{Re}(f_{CM2}) \right) / N_{12} \right| \tag{58}$$

Here $|f(t)|$ represents absolute value of function $f(t)$ and N is the normalization constant defined as;

$$N_{12} = 1.5(a_1^3 - a_2^3) \tag{59}$$

S_{12} is a measure of separability of species 1 from 2. Also S is defined as a piecewise function that becomes zero when both particles' CM factors have the same sign or when one of them is less than 0.05. Thereby, the best condition to separate and capture cells can be determined. In figure 4.8, the separability map of Jurkat and B16 cells is given. According to the figure the optimum condition for cell separation is at a medium conductivity of 0.0677 S/m and field frequency of 0.277 MHz. The highest medium
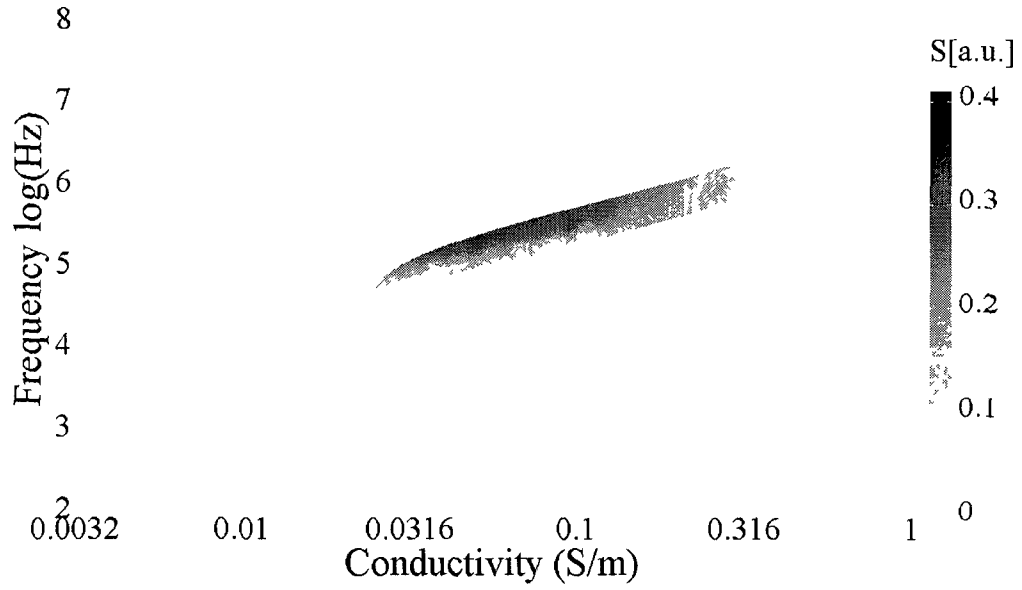
Figure 0.8 Separability parameter for Jurkat and B16 cells

conductivity to achieve efficient cell separation is at 0.44 S/m and 3.22 MHz; however, the cell separability at this conductivity is 10 times lower than the separability at 0.0677 S/m as can be seen from the contour values. The power dissipation of such a highly conductive medium will also be higher, lowering the energy allocated for dielectrophoretic particle separation. In addition to power dissipation, the electrothermal motion, which is due to joule heating in the chamber, will be disruptive to cell separation at higher conductivities. Consequently, higher conductivity media should be avoided for cell separation. The CM factors of B16 and Jurkat cells at medium conductivity of 0.0681 S/m and 0.44 S/m are plotted in figure 4.9 (a) and (b), respectively. The separability of blood cells and epithelial based tumor cells is crucial for biomedical applications that require dielectrophoretic separation of circulating tumor cells from peripheral blood cells. The highest conductivity values at which separation is achievable might be used to determine the dilution rate of a raw sample. For instance, blood that has a conductivity of ~1.5 S/m should be diluted about 22 times by low conductive buffer in order to reach

0.0681 S/m conductivity. This affects overall volume of the buffer. The 22 fold increase in the sample volume can be a challenge for direct separation of cancer cells from whole blood.
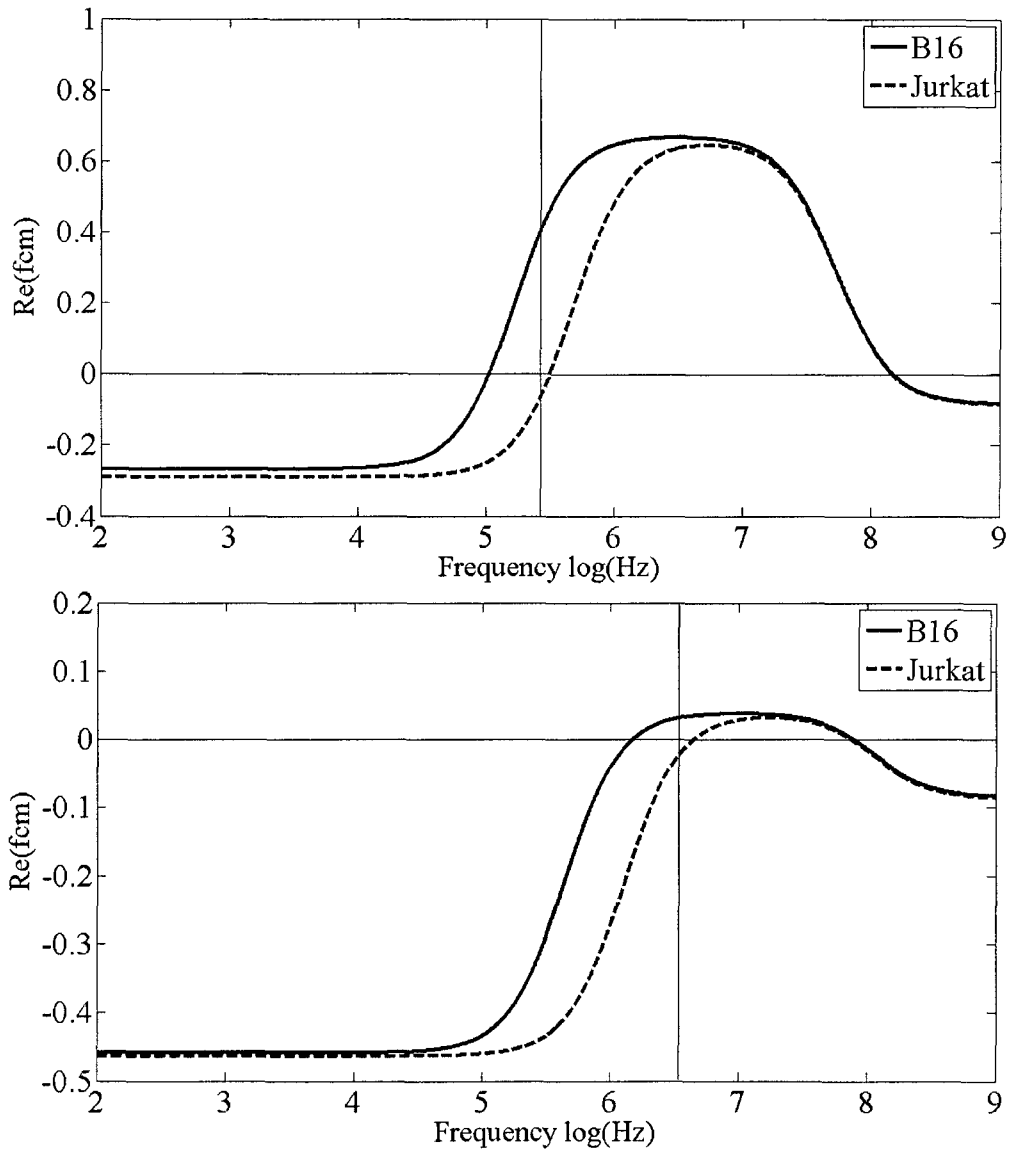

Figure 0.9 Real part of the CM factor for Jurkat and B16 cells at 0.068 S/m (a) and 0.44 S/m (b) medium conductivity

CHAPTER 5

CONCLUSIONS

A microfluidic device to measure dielectric properties of cells is investigated in this dissertation. The device consists of parallel plates of gold electrodes separated by a PDMS microfluidic channel. The chamber in the middle of the microfluidic channel holds around 5 µl of cell suspension, which corresponds to 50,000 cells at 5% volume fraction for an average cell of 10 µm radius. Usually conventional devices for dielectric spectroscopy require cell suspension volumes on the order of milliliters, which in turn is costly. Such reduced volumes are effective in lowering cost, especially for primary cells. The device investigated in this study can operate with such reduced volumes compared to conventional devices that hold up to milliliters of fluids. In addition, materials constituting the device are cheap.

Jurkat, B16F10, and chondrocyte cells membrane capacitance and conductance are measured using the microfluidic device. The measurement routine uses a combination of constant phase element, Maxwell-Wagner mixture, and single shell models to represent electrode polarization, cell suspension, and single cells, respectively. These three cells differ in their origin and function in the body. Among them chondrocyte cells have the largest membrane capacitance and conductance. The high capacitance of chondrocyte cells suggest morphologically rich cell surface. Chondrocyte cells are capable of forming an extracellular matrix, and in the body they do not stay in contact. They respond to external osmolarity and pH changes by their high number of membrane transporters. High membrane conductance affirms the existence of a high number of membrane transporters. The low resistive tangential pathways around the cell can also contribute

to high membrane conductance of chondrocyte cells, suggesting high zeta potential. The dielectric responses of Jurkat and chondrocyte cells are also recorded against changing osmolarity. Jurkat cells exhibit osmotic swelling and decrease in cell membrane capacitance and conductance as the buffer osmolarity is decreased. The decrease in cell membrane capacitance is consistent with osmotic swelling as the cell membrane unfolds, flattens, and charge-holding capacity decreases. In contrast, chondrocyte cells did not exhibit osmotic swelling at the same osmolarity range. This suggests that either the isotonic conditions in this study are already hypotonic for the chondrocyte cells or chondrocyte cells undergo a regulatory volume decrease in the time course of the experiment. The ionic efflux from Hepa cells that are suspended in low conductivity buffer is quantified using the single shell model. The ionic flux from an average cell is quantified by measuring extracellular conductivity versus time.

The main drawback of the measurement routine used in this study is that multiple solution sets minimize the residual between measurement and model data. In order to overcome this issue only membrane capacitance and conductance out of 5 cell parameters were set to change in the routine, and also DEP crossover measurements are employed for verification.

A separability parameter is introduced in the last part of the results section. The separability parameter depends on the CM factor differences between the two cells, and uses their dielectric parameters as input. Selection of the optimum parameters for cell separation is possible by plotting the separability parameter against the buffer conductivity and field frequency. Utilization of the separability parameter will yield efficient and faster cell separation devices using DEP. Separability parameter for B16 and

Jurkat cell pair is calculated in this study. Optimum buffer conductivity and field frequency are stated as cell separation conditions for B16 and Jurkat cell pair.

A major application of the microfluidic dielectric spectroscopy is in quantitative biology. Rapid, precise, and low cost measurement of cells by dielectric spectroscopy will enable researchers to explore single cell dynamics in the future. These observations can be used to understand the complex nature of cells or to develop effective therapies against disorders. In addition, biomedical usage of DEP and microfluidic dielectric spectroscopy is prominent. Circulating tumor cells in peripheral blood can be captured by DEP and further analyzed by dielectric spectroscopy. These applications might be suitable in minimum residual disease screening as well. Microfluidic cell cytometry might replace conventional flow cytometers soon, as they readily provide accurate information. However, the low throughput of microfluidic systems still remains as a problem to solve.

CHAPTER 6

FUTURE WORK

Future studies of microfluidic dielectric spectroscopy of cells should include real time observation of cells under a microscope. This will allow additional measurements such as size and volume fraction measurements that are critical while determining the cell dielectric properties. Exact determination of volume fraction and size will improve modeling of the dielectric response. In addition, viability assays or other fluorescent based studies, such as calcium release, can be performed simultaneously with dielectric measurements. Cells are affected during subsequent washing steps between experiments or at the onset of an experiment, which in turn cause errors in the measurement. A system that can hold the cells while a buffer washes them can eliminate these measurement errors. In addition, the same group of cells could be probed as the surrounding buffer is changed, which would decrease the statistical fluctuation in their response. An improved device would be able to trap and measure single cell dielectric response. Thereby, the merits of single cell measurements could be achieved. On the other hand, optimization algorithm used to derive cell parameters can be changed to find local and global minimums. A good add-on to a single cell measurement device would be a mechanism to dynamically load and unload single cells. Large numbers of cells can be probed simultaneously in a large number of single cell trapping sites by using this mechanism. A futuristic approach would be utilization of nano-electrodes (either floating or stationary) to map the dielectric response of a single cell's interior or exterior.

REFERENCES

ASAMI, K., YONEZAWA, T., WAKAMATSU, H. & KOYANAGI, N. 1996. Dielectric spectroscopy of biological cells. *Bioelectrochemistry and Bioenergetics,* 40, 141-145.

BALAKRISNAN, B., PATIL, S. & SMELA, E. 2009. Patterning PDMS using a combination of wet and dry etching. *Journal of Micromechanics and Microengineering,* 19, 047002.

BECKER, F. F. & ET AL. 1994. The removal of human leukaemia cells from blood using interdigitated microelectrodes. *Journal of Physics D: Applied Physics,* 27, 2659.

BERNABINI, C., HOLMES, D. & MORGAN, H. 2011. Micro-impedance cytometry for detection and analysis of micron-sized particles and bacteria. *Lab on a Chip,* 11, 407-412.

BHATTACHARYA, S., DATTA, A., BERG, J. M. & GANGOPADHYAY, S. 2005. Studies on surface wettability of poly (dimethyl) siloxane (PDMS) and glass under oxygen-plasma treatment and correlation with bond strength. *Microelectromechanical Systems, Journal of,* 14, 590-597.

BORDI, F., CAMETTI, C. & GILI, T. 2001. Reduction of the contribution of electrode polarization effects in the radiowave dielectric measurements of highly conductive biological cell suspensions. *Bioelectrochemistry,* 54, 53-61.

BURT, J. P. H., PETHIG, R., GASCOYNE, P. R. C. & BECKER, F. F. 1990. Dielectrophoretic characterisation of Friend murine erythroleukaemic cells as a measure of induced differentiation. *Biochimica et Biophysica Acta (BBA)-General Subjects,* 1034, 93-101.

CARSTENSEN, E. 1967. Passive Electrical Properties of Microorganisms II. Resistance of the Bacterial Membrane. *Biophysical journal,* 7, 493-503.

CARSTENSEN, E. & MARQUIS, R. 1968. Passive Electrical Properties of Microorganisms III. Conductivity of Isolated Bacterial Cell Walls. *Biophysical journal,* 8, 536-548.

CHEN, J. 2011. A microfluidic device for simultaneous electrical and mechanical measurements on single cells. *Biomicrofluidics,* 5, 014113.

CHENG, I.-F., CHANG, H.-C., HOU, D. & CHANG, H.-C. 2007. *An integrated dielectrophoretic chip for continuous bioparticle filtering, focusing, sorting, trapping, and detecting*, AIP.

CHIA-FU, C. & ZENHAUSERN, F. 2003. Electrodeless dielectrophoresis for micro total analysis systems. *Engineering in Medicine and Biology Magazine, IEEE,* 22, 62-67.

CHO, Y., KIM, H. S., FRAZIER, A. B., CHEN, Z. G., SHIN, D. M. & HAN, A. 2009. Whole-Cell Impedance Analysis for Highly and Poorly Metastatic Cancer Cells *Journal Microelectromechanical Systems,* 18, 808-816.

CHO, Y. H., YAMAMOTO, T., SAKAI, Y., FUJII, T. & BEOMJOON, K. 2006. Development of microfluidic device for electrical/physical characterization of single cell. *Microelectromechanical Systems, Journal of,* 15, 287-295.

CLARKE, R. & GREGORY, A. 2003. A Guide to the characterisation of dielectric materials at RF and microwave frequencies. *The Institute of Measurement and Control (IMC) and National Physical Laboratory (NPL), London, ISBN 0,* 904457, 9.

COULTER, W. H. Year. High speed automatic blood cell counter and cell size analyzer. *In,* 1956.

CURRIE, I. G. 2002. *Fundamental Mechanics of Fluids* CRC Press.

DESAI, S. P., TAFF, B. M. & VOLDMAN, J. 2007. A photopatternable silicone for BioMEMS applications. *Proc. Micro Total Anal. Syst.(μ-TAS,* 448–450.

DHARIA, S., AYLIFFE, H. E. & RABBITT, R. D. 2009. Single cell electric impedance topography: Mapping membrane capacitance. *Lab Chip,* 9, 3370-3377.

DI BIASIO, A., AMBROSONE, L. & CAMETTI, C. 2010. The Dielectric Behavior of Nonspherical Biological Cell Suspensions: An Analytic Approach. *Biophysical journal,* 99, 163-174.

DI BIASIO, A. & CAMETTI, C. 2010a. d-glucose-induced alterations in the electrical parameters of human erythrocyte cell membrane. *Bioelectrochemistry,* 77, 151-157.

DI BIASIO, A. & CAMETTI, C. 2010b. Polarizability of spherical biological cells in the presence of localized surface charge distributions at the membrane interfaces. *Physical Review E,* 82, 021917.

DYKE, C. A. & TOUR, J. M. 2004. Covalent functionalization of single-walled carbon nanotubes for materials applications. *The Journal of Physical Chemistry A,* 108, 11151-11159.

ERMOLINA, I., POLEVAYA, Y., FELDMAN, Y., GINZBURG, B. & SCHLESINGER, M. 2001. Study of normal and malignant white blood cells by time domaindielectric spectroscopy. *IEEE Transactions on Dielectrics and Electrical Insulation,* 8, 253-261.

FELDMAN, Y., POLYGALOV, E., ERMOLINA, I., POLEVAYA, Y. & TSENTSIPER, B. 2001. Electrode polarization correction in time domain dielectric spectroscopy. *Measurement Science and Technology,* 12, 1355-64.

FETTIPLACE, R., ANDREWS, D. M. & HAYDON, D. A. 1971. The thickness, composition and structure of some lipid bilayers and natural membranes. *Journal of Membrane Biology,* 5, 277-296.

FOSTER, K. R. & SCHWAN, H. P. 1989. Dielectric properties of tissues and biological materials: a critical review. *Critical Reviews in Biomedical Engineering,* 17, 25-104.

FRICKE, H. 1924. A Mathematical Treatment of the Electric Conductivity and Capacity of Disperse Systems I. The Electric Conductivity of a Suspension of Homogeneous Spheroids. *Physical Review,* 24, 575.

FRICKE, H. & MORSE, S. 1925. The electric resistance and capacity of blood for frequencies between 800 and 4½ million cycles. *The Journal of General Physiology,* 9, 153.

FROUDE, V. E., GODFROY, J. I., WANG, S., DOMBEK, H. & ZHU, Y. 2010. Anomalous Dielectrophoresis of Nanoparticles: A Rapid and Sensitive Characterization by Single-Particle Laser Spectroscopy. *The Journal of Physical Chemistry C,* 114, 18880-18885.

GARNER, A. L., CHEN, G., CHEN, N., SRIDHARA, V., KOLB, J. F., SWANSON, R. J., BEEBE, S. J., JOSHI, R. P. & SCHOENBACH, K. H. 2007. Ultrashort electric pulse induced changes in cellular dielectric properties. *Biochemical and Biophysical Research Communications,* 362, 139-144.

GASCOYNE, P. R. C., PETHIG, R., BURT, J. P. H. & BECKER, F. F. 1993. Membrane changes accompanying the induced differentiation of Friend murine erythroleukemia cells studied by dielectrophoresis. *Biochimica et Biophysica Acta (BBA)-Biomembranes,* 1149, 119-126.

GASCOYNE, P. R. C., WANG, X.-B., HUANG, Y. & BECKER, F. F. 1997. Dielectrophoretic Separation of Cancer Cells from Blood. *IEEE Tansactions on Industry Applications,* 33, 670-678.

GOU, H.-L., ZHANG, X.-B., BAO, N., XU, J.-J., XIA, X.-H. & CHEN, H.-Y. 2011. Label-free electrical discrimination of cells at normal, apoptotic and necrotic status with a microfluidic device. *Journal of Chromatography A,* 1218, 5725-5729.

GRACE CHAO, P., TANG, Z., ANGELINI, E., WEST, A. C., COSTA, K. D. & HUNG, C. T. 2005. Dynamic osmotic loading of chondrocytes using a novel microfluidic device. *Journal of Biomechanics,* 38, 1273-1281.

GREEN, N. G. & MORGAN, H. 1998. Dielectrophoresis of Submicrometer Latex Spheres. 1. Experimental Results. *The Journal of Physical Chemistry B,* 103, 41-50.

GREGORY, A. & CLARKE, R. 2007. Dielectric metrology with coaxial sensors. *Measurement Science and Technology,* 18, 1372.

GROSSE, C. & DELGADO, A. V. 2010. Dielectric dispersion in aqueous colloidal systems. *Current Opinion in Colloid & Interface Science,* 15, 145-159.

HALL, A. C., HORWITZ, E. R. & WILKINS, R. J. 1996. The cellular physiology of articular cartilage. *Experimental Physiology,* 81, 535.

HAN, A. & FRAZIER, A. B. 2006. Ion channel characterization using single cell impedance spectroscopy. *Lab on a Chip,* 6, 1412-1414.

HANAI, T. 1968. *Emulsion Science,* New York, Academic Press.

HIBINO, M., ITOH, H. & KINOSITA, K. 1993. Time courses of cell electroporation as revealed by submicrosecond imaging of transmembrane potential. *Biophysical Journal,* 64, 1789-1800.

HIBINO, M., SHIGEMORI, M., ITOH, H., NAGAYAMA, K. & KINOSITA, K. 1991. Membrane conductance of an electroporated cell analyzed by submicrosecond imaging of transmembrane potential. *Biophysical Journal,* 59, 209-220.

HONDA, M. 2009. Impedance Measurement Handbook. *A Guide to Measurement Technology and Technique.* USA: Agilent Technologies.

HUA, S. Z. & PENNELL, T. 2009. A microfluidic chip for real-time studies of the volume of single cells. *Lab on a Chip,* 9, 251-256.

HUANG, Y., HOLZER, R., PETHIG, R. & WANG, X.-B. 1999. Differences in the AC Electrodynamics of Viable and Non-viable yeast cells dtermined through combined dielectrophoresis and electrorotation studies. *Physics in Medicine and Biology,* 37, 1499-1517.

HUANG, Y., WANG, X.-B., BECKER, F. F. & GASCOYNE, P. R. C. 1996. Membrane changes associated with the temperature-sensitive P85gag-mos-dependent transformation of rat kidney cells as determined by dielectrophoresis and electrorotation. *Biochimica et Biophysica Acta (BBA) - Biomembranes,* 1282, 76-84.

HUANG, Y., WANG, X. B., HOLZEL, R., BECKER, F. & GASCOYNE, P. 1995. Electrorotational studies of the cytoplasmic dielectric properties of Friend murine erythroleukaemia cells. *Physics in Medicine and Biology,* 40, 1789.

HUNTER, R. J. 2001. *Foundations of Colloid Science,* Oxford, Oxford University Press.

ISRAELACHVILI, J. N. 2011. *Intermolecular and Surface Forces,* Burlington, Academic Press.

JANG, L.-S. & WANG, M.-H. 2007. Microfluidic device for cell capture and impedance measurement. *Biomedical Microdevices,* 9, 737-743.

JONES, T. B. 1995. *Electromechanics of Particles,* New York, Cambridge University Press.

JUSTIN, G., NASIR, M. & LIGLER, F. 2011. Hydrodynamic and electrical considerations in the design of a four-electrode impedance-based microfluidic device. *Analytical and Bioanalytical Chemistry,* 400, 1347-1358.

KAATZE, U. 1989. Complex permittivity of water as a function of frequency and temperature. *Journal of Chemical and Engineering Data,* 34, 371-374.

KAATZE, U. & FELDMAN, Y. 2006. Broadband dielectric spectrometry of liquids and biosystems. *Measurement Science and Technology,* 17, 17.

KANAGASABAPATHI, T. T., DALTON, C. & KALER, K. V. I. S. 2005. An Integrated PDMS Microfluidic Device for Dielectrophoretic Separation of Malignant Cells. *ASME Conference Proceedings,* 2005, 411-418.

KANG, Y., CETIN, B., WU, Z. & LI, D. 2009. Continuous particle separation with localized AC-dielectrophoresis using embedded electrodes and an insulating hurdle. *Electrochimica Acta,* 54, 1715-1720.

KOKLU, M., SABUNCU, A. C. & BESKOK, A. 2010. Acoustophoresis in shallow microchannels. *Journal of Colloid and Interface Science.*

KÜTTEL, C., NASCIMENTO, E., DEMIERRE, N., SILVA, T., BRASCHLER, T., RENAUD, P. & OLIVA, A. G. 2007. Label-free detection of Babesia bovis infected red blood cells using impedance spectroscopy on a microfabricated flow cytometer. *Acta Tropica,* 102, 63-68.

KUETTNER, K. E., PAULI, B. U., GALL, G., MEMOLI, V. A. & SCHENK, R. K. 1982. Synthesis of cartilage matrix by mammalian chondrocytes in vitro. I. Isolation, culture characteristics, and morphology. *The Journal of Cell Biology,* 93, 743.

LEE, S. J. J. & SUNDARARAJAN, N. 2010. *Microfabrication for Microfluidics,* Artech House Publishers.

LEVSKY, J. M. & SINGER, R. H. 2003. Gene expression and the myth of the average cell. *Trends in Cell Biology,* 13, 4-6.

LEWPIRIYAWONG, N., YANG, C. & LAM, Y. C. 2010. Continuous sorting and separation of microparticles by size using AC dielectrophoresis in a PDMS microfluidic device with 3-D conducting PDMS composite electrodes. *Electrophoresis,* 31, 2622-2631.

LI, Y., DALTON, C., CRABTREE, H. J., NILSSON, G. & KALER, K. V. I. S. 2007. Continuous dielectrophoretic cell separation microfluidic device. *Lab on a Chip,* 7, 239-248.

LYKLEMA, H. 1995. *Fundamentals of Interface and Colloid Science,* San Diego, Academic Press.

LYKLEMA, J. 2001. Surface conduction. *Journal of Physics: Condensed Matter,* 13, 5027.

MALLEO, D., NEVILL, J., LEE, L. & MORGAN, H. 2010a. Continuous differential impedance spectroscopy of single cells. *Microfluidics and Nanofluidics,* 9, 191-198.

MALLEO, D., NEVILL, J. T., VAN OOYEN, A., SCHNAKENBERG, U., LEE, L. P. & MORGAN, H. 2010b. Characterization of electrode materials for dielectric spectroscopy.

MAZZEO, B. & FLEWITT, A. 2007. Two-and four-electrode, wide-bandwidth, dielectric spectrometer for conductive liquids: Theory, limitations, and experiment. *Journal of Applied Physics,* 102, 104106.

MCDONALD, J. C., DUFFY, D. C., ANDERSON, J. R., CHIU, D. T., WU, H., SCHUELLER, O. J. A. & WHITESIDES, G. M. 2000. Fabrication of microfluidic systems in poly(dimethylsiloxane). *ELECTROPHORESIS,* 21, 27-40.

MINOR, M., VAN LEEUWEN, H. P. & LYKLEMA, J. 1998. Low-Frequency Dielectric Response of Polystyrene Latex Dispersions. *Journal of Colloid and Interface Science,* 206, 397-406.

MORGAN, H. & GREEN, N. G. 2003. *AC Electrokinetics: Colloids and Nanoparticles,* Baldock, Research Studies Press Ltd.

O'BRIEN, R. W. 1986. The high-frequency dielectric dispersion of a colloid. *Journal of Colloid and Interface Science,* 113, 81-93.

O'KONSKI, C. T. 1960. ELECTRIC PROPERTIES OF MACROMOLECULES. V. THEORY OF IONIC POLARIZATION IN POLYELECTROLYTES. *The Journal of Physical Chemistry,* 64, 605-619.

OH, S. 2008. Thick single-layer positive photoresist mold and poly (dimethylsiloxane)(PDMS) dry etching for the fabrication of a glass–PDMS–glass microfluidic device. *Journal of Micromechanics and Microengineering,* 18, 115025.

PADDISON, S. J., PAUL, R. & KALER, K. V. I. S. 1995. Hysteresis loops in the low frequency region of the Clausius-Mossotti polarization factor: the result of non-linear boundary conditions at the particle interface. *Bioelectrochemistry and Bioenergetics,* 38, 321-331.

PAKHOMOV, A., KOLB, J., WHITE, J., JOSHI, R., XIAO, S. & SCHOENBACH, K. 2007. Long lasting plasma membrane permeabilization in mammalian cells by nanosecond pulsed electric field (nsPEF). *Bioelectromagnetics,* 28, 655-663.

PARK, J., KIM, H. S. & HAN, A. 2009. Micropatterning of poly (dimethylsiloxane) using a photoresist lift-off technique for selective electrical insulation of

microelectrode arrays. *Journal of Micromechanics and Microengineering,* 19, 065016.

PARK, S., ZHANG, Y., WANG, T.-H. & YANG, S. 2011. Continuous dielectrophoretic bacterial separation and concentration from physiological media of high conductivity. *Lab on a Chip,* 11, 2893-2900.

PETHIG, R. 1979. *Dielectric and Electronic Properties of Biological Materials,* Surrey, John Wiley & Sons, Ltd.

PETHIG, R. 2010. Dielectrophoresis: Status of the theory, technology, and applications. *Biomicrofluidics,* 4, 022811-35.

PETHIG, R., BRESSLER, V., CARSWELL-CRUMPTON, C., CHEN, Y., FOSTER-HAJE, L., GARCÍA-OJEDA, M. E., LEE, R. S., LOCK, G. M., TALARY, M. S. & TATE, K. M. 2002. Dielectrophoretic studies of the activation of human T lymphocytes using a newly developed cell profiling system. *ELECTROPHORESIS,* 23, 2057-2063.

PETHIG, R. & ET AL. 1992. Positive and negative dielectrophoretic collection of colloidal particles using interdigitated castellated microelectrodes. *Journal of Physics D: Applied Physics,* 25, 881.

PETHIG, R., JAKUBEK, L., SANGER, R., HEART, E., CORSON, E. & SMITH, P. J. S. Year. Electrokinetic measurements of membrane capacitance and conductance for pancreatic β-cells. *In,* 2005. IET, 189-193.

PETHIG, R. & KELL, D. B. 1987. The passive electrical properties of biological systems: their significance in physiology, biophysics and biotechnology. *Physics in Medicine and Biology,* 32, 933.

PETHIG, R. & TALARY, M. S. 2007. Dielectrophoretic detection of membrane morphology changes in Jurkat T-cells undergoing etoposide-induced apoptosis. *IET Nanobiotechnology,* 1, 2-9.

POHL, H. A. 1951. The Motion and Precipitation of Suspensoids in Divergent Electric Fields. *Journal of Applied Physics,* 22, 869-871.

POLEVAYA, Y., ERMOLINA, I., SCHLESINGER, M., GINZBURG, B.-Z. & FELDMAN, Y. 1999a. Time domain dielectric spectroscopy study of human cells: II. Normal and malignant white blood cells. *Biochimica et Biophysica Acta (BBA) - Biomembranes,* 1419, 257-271.

POLEVAYA, Y., ERMOLINA, I., SCHLESINGER, M., GINZBURG, B. Z. & FELDMAN, Y. 1999b. Time domain dielectric spectroscopy study of human cells:: II. Normal and malignant white blood cells. *Biochimica et Biophysica Acta (BBA)-Biomembranes,* 1419, 257-271.

PRODAN, C. & PRODAN, E. 1999. The dielectric behaviour of living cell suspensions. *Journal of Physics D: Applied Physics,* 32, 335.

PRODAN, E., PRODAN, C. & MILLER, J. H. 2008. The Dielectric Response of Spherical Live Cells in Suspension: An Analytic Solution. *Biophysical Journal,* 95, 4174-4182.

REICHLE, C., MULLER, T., SCHNELLE, T. & FUHR, G. 1999. Electro-rotation in octopole micro cages. *Journal of Physics D: Applied Physics,* 32, 2128.

SABUNCU, A. C., LIU, J. A., BEEBE, S. J. & BESKOK, A. 2010. Dielectrophoretic separation of mouse melanoma clones. *Biomicrofluidics,* 4, 021101-7.

SALEH, O. A. & SOHN, L. L. 2003. An artificial nanopore for molecular sensing. *Nano Letters,* 3, 37-38.

SCHADE-KAMPMANN, G., HUWILER, A., HEBEISEN, M., HESSLER, T. & DI BERARDINO, M. 2008. On-chip non-invasive and label-free cell discrimination by impedance spectroscopy. *Cell Proliferation,* 41, 830-840.

SCHNELLE, T., MÜLLER, T., GRADL, G., SHIRLEY, S. G. & FUHR, G. 1999. Paired microelectrode system: dielectrophoretic particle sorting and force calibration. *Journal of Electrostatics,* 47, 121-132.

SIKANEN, T., TUOMIKOSKI, S., KETOLA, R. A., KOSTIAINEN, R., FRANSSILA, S. & KOTIAHO, T. 2005. Characterization of SU-8 for electrokinetic microfluidic applications. *Lab Chip,* 5, 888-896.

SPENCER, D. & MORGAN, H. 2011. Positional dependence of particles in microfludic impedance cytometry. *Lab Chip.*

SPILLER, D. G., WOOD, C. D., RAND, D. A. & WHITE, M. R. H. 2010. Measurement of single-cell dynamics. *Nature,* 465, 736-745.

STANGEGAARD, M., WANG, Z., KUTTER, J. P., DUFVA, M. & WOLFF, A. 2006. Whole genome expression profiling using DNA microarray for determining biocompatibility of polymeric surfaces. *Mol. BioSyst.,* 2, 421-428.

STONEMAN, M., CHATURVEDI, A., JANSMA, D. B., KOSEMPA, M., ZENG, C. & RAICU, V. 2007. Protein influence on the plasma membrane dielectric properties: In vivo study utilizing dielectric spectroscopy and fluorescence microscopy. *Bioelectrochemistry*, 70, 542-550.

SUKHORUKOV, V., ARNOLD, W. & ZIMMERMANN, U. 1993. Hypotonically induced changes in the plasma membrane of cultured mammalian cells. *Journal of Membrane Biology*, 132, 27-40.

TALARY, M., MILLS, K., HOY, T., BURNETT, A. & PETHIG, R. 1995. Dielectrophoretic separation and enrichment of CD34+cell subpopulation from bone marrow and peripheral blood stem cells. *Medical and Biological Engineering and Computing*, 33, 235-237.

THEIN, M., ASPHAHANI, F., CHENG, A., BUCKMASTER, R., ZHANG, M. & XU, J. 2010. Response characteristics of single-cell impedance sensors employed with surface-modified microelectrodes. *Biosensors and Bioelectronics*, 25, 1963-1969.

UNGER, M. A., CHOU, H. P., THORSEN, T., SCHERER, A. & QUAKE, S. R. 2000. Monolithic microfabricated valves and pumps by multilayer soft lithography. *Science*, 288, 113.

VAN DER WAL, A., MINOR, M., NORDE, W., ZEHNDER, A. J. B. & LYKLEMA, J. 1997. Conductivity and Dielectric Dispersion of Gram-Positive Bacterial Cells. *Journal of Colloid and Interface Science*, 186, 71-79.

WANG, W., FOLEY, K., SHAN, X., WANG, S., EATON, S., NAGARAJ, V. J., WIKTOR, P., PATEL, U. & TAO, N. 2011. Single cells and intracellular processes studied by a plasmonic-based electrochemical impedance microscopy. *Nature Chemistry*, 3, 251-257.

WANG, X.-B., HUANG, Y., GASCOYNE, P., BECKER, F. F., HOELZEL, R. & PETHIG, R. 1994. Changes in Friend murine erythroleukemia cell membranes during induced differentiation dtermined by electrorotation. *Biochimica et Biophysica Acta (BBA)-Biomembranes*, 1993, 330-334.

WANG, X., BECKER, F. F. & GASCOYNE, P. R. C. 2002. Membrane dielectric changes indicate induced apoptosis in HL-60 cells more sensitively than surface phosphatidylserine expression or DNA fragmentation. *Biochimica et Biophysica Acta*, 1564, 412-420.

WANG, X., WANG, X.-B. & GASCOYNE, P. R. C. 1997. General expressions for dielectrophoretic force and electrorotational torque derived using the Maxwell stress tensor method. *Journal of Electrostatics*, 39, 277-295.

WU, X., KANG, Y., WANG, Y. N., XU, D. & LI, D. 2008. Microfluidic differential resistive pulse sensors. *Electrophoresis,* 29, 2754-2759.

YANG, F., YANG, X., JIANG, H., BULKHAULTS, P., WOOD, P., HRUSHESKY, W. & WANG, G. 2010. Dielectrophoretic Separation of Colorectal Cancer Cells, Biomicrofluidics, 4, 0132041-13.

YANG, J., HUANG, Y., WANG, X., WANG, X.-B., BECKER, F. F. & GASCOYNE, P. R. C. 1999. Dielectric Properties of Human Leukocyte Subpopulations Determined by Electrorotation as a Cell Separation Criterion. *Biophysical journal,* 76, 3307-3314.

ZHANG, H., CHON, C. H., PAN, X. & LI, D. 2009. Methods for counting particles in microfluidic applications. *Microfluidics and Nanofluidics,* 7, 739-749.

ZHAO, H. & BAU, H. H. 2010. Polarization of Nanorods Submerged in an Electrolyte Solution and Subjected to an ac Electrical Field. *Langmuir,* 26, 5412-5420.

ZHUANG, J., BALDWIN, W. H., SCHOENBACH, K. H. & KOLB, J. F. 2009. Pulsed Electric Field Induced Changes in Dielectric Properties of Biological Cells. *Pulsed Power Conference.* Washington, DC.

ZHURAVEL, D. & KAERN, M. 2005. Physics takes another stab at biological design principles. *Mol Syst Biol,* 1.

VITA

Ahmet Can Sabuncu

Aerospace Engineering Department

Old Dominion University

Norfolk, VA 23529

Educational Background

Ph.D. : December 2011, Old Dominion University, Norfolk VA USA

Major : Aerospace Engineering

Dissertation : A Microfluidic Device for Impedance Spectroscopy

M.Sc. : June 2007, Istanbul Technical University, Istanbul TURKEY

Major : Aeronautical Engineering

Thesis : Aeroacoustics of Vehicle Side Mirrors

B.Sc. : June 2005, Yildiz Technical University, Istanbul TURKEY

Major : Mechanical Engineering

Thesis : Road Vehicle Aerodynamics

Major Publications

1. Sabuncu, A.C., Kalluri, B.S., Qian, S., Stacey, M., Beskok, A., "Dispersion state and toxicity of mwCNTs in cell culture medium with different T80 concentrations" *Colloids and Surfaces B:Biointerfaces*, 78(1): pp 36-43, 2010.

2. Sabuncu, A.C., Liu, J.A., Beebe, S.J., and Beskok, A., "Dielectrophoretic separation of mouse melanoma clones" *Biomicrofluidics*, 4: pp 021101 1-7, 2010.

3. Koklu M., Sabuncu A.C., and Beskok A., "Acoustophoresis in shallow microchannels", *Journal of Colloid and Interface Science*, 351(2): pp 407:414, 2010.

4. Sabuncu, A.C., Grubbs, J., Qian, S., Abdel-Fattah T. M., Stacey, M., Beskok, A., "Probing nanoparticle interactions in cell culture media" (*Submitted*)